Single Atom Catalysts-Enabled Catalytic Ammonia Combustion at Above 1000°C

Yankun Du,[1,†] Bingqing Yao,[1,†] Liang Xu,[1] Shangchen Lu,[1] Chaokai Xu,[1] Peijie Han[2], Sheng Dai,[3] Sikai Wang,[2] Shibo Xi,[4] Ning Yan[2,5*] and Qian He[1,5*]

1 Department of Material Science and Engineering, College of Design and Engineering, National University of Singapore, 9 Engineering Drive 1, EA #03-09, Singapore, 117575w

2 Department of Chemical and Biomolecular Engineering, College of Design and Engineering, National University of Singapore, 4 Engineering Drive 4, E5 #02-29, Singapore, 117585

3 Key Laboratory for Advanced Materials and Joint International Research Laboratory of Precision Chemistry and Molecular Engineering, School of Chemistry and Molecular Engineering, East China University of Science & Technology, Shanghai 200237, China

4 Institute of Sustainability for Chemicals, Energy and Environment (ISCE2), Agency for Science, Technology and Research in Singapore (A∗STAR), 1 Pesek Road, Jurong Island 627833, Singapore

5 Centre for Hydrogen Innovations, National University of Singapore, E8, 1 Engineering Drive 3, Singapore, 117580

*Corresponding authors: Ning Yan (NY) ning.yan@nus.edu.sg; Qian He (QH): heqian@nus.edu.sg

† These authors contributed equally.

ABSTRACT

Green NH_3 is a promising renewable fuel but suffers from having poor combustion characteristics. High-temperature catalytic ammonia combustion (HT-CAC) provides an attractive solution to improve the combustibility of NH_3 and allows high-quality heat to be extracted with reduced harmful emissions. Achieving HT-CAC is a difficult task due to (i) demanding stability requirements for catalysts and (ii) potentially high NO_x emissions. Here, we report that atomically dispersed Pt on 10%ZrO_2-Al_2O_3 can facilitate the HT-CAC process. The catalyst ignites NH_3 combustion just above 200 °C and has excellent stability when operated at 1100 °C. The presence of the catalyst also reduces the NO_x emission to around 50 ppm without detectable NH_3 slip. This work shows that combining single atom catalysts with refractory support materials is an effective strategy for designing catalysts for HT-CAC, which will in turn help to decarbonize many "hard-to-abate" sectors such as industrial heating.

INTRODUCTION

Combustion has been and still is our primary method for producing energy. It reliably outputs high-temperature and high-flux heat on demand, providing us with the versatility to fulfil almost all kinds of energy needs either directly or indirectly. Many key sectors, such as the production of steel, glass, and cement, as well as heavy-duty transportation, are deeply anchored to fossil fuel combustion and have few viable alternatives. Greenhouse gas (GHG) emissions from these sectors are considered "hard-to-abate," posing significant challenges to achieving a "net-zero" future.[1-3] To put the scale of the challenge into perspective, just the production of heat in heavy industry accounts for about 10% of global CO_2 emissions,[4,5] a figure surpassing the emissions from all cars combined. To transition towards sustainability and continue to harness the benefits offered by combustion, developing renewable combustion fuels and associated technologies is needed.[5-7]

Ammonia (NH_3), which can be made from air, water, and renewable energy, is a promising candidate for such a renewable combustion fuel. It offers high energy density (12.7 MJ/L), excellent stability, and a long history of large-scale production and utilization.[8-11] Several potential renewable energy-exporting[12,13] and importing[14,15] countries are actively investing in NH_3-based renewable energy infrastructures.[16,17] Yet, NH_3 combustion presents its own set of challenges: Firstly, NH_3 has poor combustion characteristics, marked by a narrow flammable range for an NH_3/air mixture, high ignition temperature, and slow flame speed.[18,19] Current solutions, like co-firing NH_3 with conventional fuels or hydrogen (**Figure 1A**), either undermine its carbon-neutral potential or necessitate the development of large-scale NH_3 crackers.[20] In addition, directly burning NH_3 often results in high NO_x emissions (*e.g.*, thousands of parts per million (ppm)[21]), which can be challenging to mitigate with existing current deNO_x technologies.

Catalytic ammonia combustion (CAC) provides a solution by facilitating the combustion reaction and reducing both fuel-derived and thermal-induced NO_x, especially considering NH_3 serves as the reductant in the selective (non) catalytic reduction (SNCR or SCR) of NO_x.[22-24] However, most previous works on CAC were carried out in the context of nitric acid production[25] or pollution-control,[26,27] and thus not directly related to energy production. Some studied the combustion of NH_3-containing biogas,[28-32] where CAC was investigated in the fuel-lean conditions. In those cases, high NO_x emissions were the main concern, which can be somewhat reduced at higher reaction temperatures

(> 750°C) and with the presence of reductants such as CO and NH_3. For energy harvesting from ammonia combustion, some pioneering work was carried out by Machida and colleagues,[33-41] who investigated various oxides and supported metal catalysts for CAC up to 900°C (**Figure 1B**). In their works, relatively low NO_x emissions were achieved either at lower combustion temperatures (*e.g.*, around 600°C[33]) or at undesired fuel-rich conditions[41] (air-to-fuel ratio $\lambda < 1$). The relatively low combustion temperatures will limit the thermal efficiency and the application scope of CAC, making it not suitable for processes that require higher temperatures approaching or above 1000°C (*e.g.*, steam cracking, smelting)

Herein, we report high-temperature (1100°C) catalytic ammonia combustion (HT-CAC) under fuel-lean conditions (*i.e.*, air-to-fuel ratio $\lambda = 1.5$, and 1 represents a stoichiometric ratio). Our best catalyst, 0.5%Pt/10%ZrO_2-Al_2O_3 (denoted as 0.5Pt/10ZrAl) ignites NH_3 combustion at a temperature of about 215°C. It also exhibits excellent thermal stability and keeps fully operational after long-term reaction at 1100°C. In addition, this HT-CAC process can effectively lower the NO_x emission and achieve a NO_x concentration of around 50 ppm. Our experimental evidence suggested that atomically dispersed Pt species were responsible for the combination of excellent activity, selectivity, and stability in the catalytic combustion reaction. We thus show that this single-atom-enabled, HT-CAC is a feasible way of extracting high-quality heat from NH_3 while minimizing harmful emissions (**Figure 1C**).

RESULTS AND DISCUSSIONS

0.5Pt/10ZrAl identified as an effective catalyst for HT-CAC

The oxidation of NH_3 involves a rather complex reaction network with different nitrogen containing compounds (**Figure S1**). There are at least three key reactions:[22,26] (R1) selective oxidation of NH_3 to N_2 and H_2O, our desired pathway; (R2) oxidation of NH_3 to NO, essential in the Ostwald process, which operates at relatively high temperatures (*e.g.*, 600-900°C); and (R3) selective catalytic reduction of NO using NH_3. NH_3 could also undergo decomposition to form H_2, followed by H_2 combustion to water. At high temperature, these reactions likely take place both at the surface of the catalysts and in the gas phase. Note that, if the combustion temperature is kept below 1300°C, the formation of thermal-induced NO_x from N_2 is usually minimum.[42]

$$4NH_3(g) + 3O_2(g) \rightarrow 2N_2(g) + 6H_2O(g) \quad (R1)$$

$$\Delta H_{298K} = -1266 \text{ kJ mol}^{-1}$$

$$4NH_3(g) + 5O_2(g) \rightarrow 4NO(g) + 6H_2O(g) \quad (R2)$$

$$\Delta H_{298K} = -904 \text{ kJ mol}^{-1}$$

$$4NO(g) + 4NH_3(g) + O_2(g) \rightarrow 4N_2(g) + 6H_2O(g) \quad (R3)$$

$$\Delta H_{298K} = -1628 \text{ kJ mol}^{-1}$$

Our vision for a suitable catalyst for HT-CAC should have the following characteristics: (i) a good low-temperature NH_3 oxidation activity to "ignite" the fuel-air mixture (*i.e.*, a low light-off temperature); (ii) robust structural stability and (iii) high N_2 selectivity to ensure low NO_x emission at the desired high operating temperatures (*e.g.*, >1000°C). In this context, we speculate that single-atom catalysts (SACs) supported on high-surface-area, refractory materials may offer a promising solution. SACs are renowned for their excellent thermal stability under oxidative conditions,[43-45] although few instances are currently known to us where SACs have been applied at temperatures above 1000°C. To find a suitable catalyst for HT-CAC, we tested various materials using a fixed-bed reactor (**Figures S2A** and **S2B**). In a typical experiment, a non-explosive mixture of 2 vol.% NH_3 and 3 vol.% O_2, balanced with Ar, was supplied to the catalyst bed with a total flow rate of 100 ml/min. The catalyst bed contained 200 mg of catalyst (~0.4 ml) mixed with 1200 mg of quartz sand (50-70 mesh, Sigma-Aldrich), yielding a catalyst weight-to-flow ratio (W/F) of 2×10^{-3} (g min)/ml. The gas lines were heated to avoid condensation, and the combustion products at any given temperature were analysed using a mass spectrometer. (see **Supplementary Information** for more details). The catalyst bed was heated from room temperature to 1100°C, with a ramp rate of 1°C/min between 200-300°C and 10°C/min thereafter, followed by a 4-hours (or more) at 1100°C. Upon reaching 1100°C, it took approximately 30 minutes for the top surface of the catalyst bed to reach a steady-state temperature of around 1095°C (**Figures S2C** and **S2D**). All reported temperatures refer to nominal furnace temperatures unless specified otherwise.

Initial HT-CAC tests with Al_2O_3, ZrO_2, quartz sands, or an empty tube showed NH_3 ignition (T_{10}) at ~500°C, with 100% NH_3 conversion achieved at 1100°C, likely due to homogeneous gas-phase reactions. NO_x emissions initially peaked at around 100 ppm but stabilised at 14~75 ppm after 1 hour (**Table S1, entries 1-4**).

Among tested materials, 10% ZrO_2- Al_2O_3 (10ZrAl) exhibited excellent thermal stability and good N_2 selectivity at 1100°C (**Table S1, entries 5** and **6**). Loading 0.5 wt% Pt (0.5Pt/10ZrAl) significantly improved low-temperature performance, reducing T_{10} and T_{90} from ~500–600°C to <300°C (**Figure 2A**, **Table S1**, **entries 7-9**). Fresh 0.5Pt/10ZrAl, however, initially showed low N_2 selectivity (< 80%) and high NO_x emissions (>2000 ppm) at 1100°C, which stabilised to about 30 ppm after 1 hour. Intriguingly, when the used 0.5Pt/10ZrAl catalyst was recycled and reused in HT-CAC, the initial NO_x emission spike was eliminated. Its performance also improved: T_{90} decreased to ~215°C, and N_2 selectivity at 1100°C exceeded 99%, resulting in NO_x emissions below 40 ppm (**Figure 2B**). This indicates that the 0.5Pt/10ZrAl catalyst undergoes *in situ* activation during its first HT-CAC run at 1100°C.

To evaluate long-term stability under HT-CAC conditions, the 0.5Pt/10ZrAl-usedx1 catalyst was subjected to multiple 10-hour runs at 1100°C. As shown in **Figure S3**, the catalyst consistently achieved 100% NH_3 conversion and maintained low NO_x emissions throughout each 10-hour run. Upon reuse, the T_{90} remained stable at about 223°C. Light-off curves for eight consecutive 10-hour cycles (**Figure 2C**) demonstrated that T_{90} stayed below 250°C, while NO_x emissions (**Figure 2D**) remained consistently low, around 50 ppm.

Under our standard test conditions, Ar was used as the balancing gas to accurately evaluate the N_2 selectivity of the combustion catalysts. Since practical combustion will likely use air, which contains a large amount of N_2, additional HT-CAC experiments were conducted with N_2 as the balancing gas. Starting from the fresh catalysts, the results of the 2nd HT-CAC experiment were presented in **Figures 2E**, **2F**, **S4**, and **Table S2**, as we expect catalysts to be activated after the 1st run of HT-CAC. The bare support (10ZrAl), quartz sand, and an empty tube exhibited high T_{10} values at around 500°C, whereas 0.5%Pt/10ZrAl exhibited T_{10} values at around 300°C. The importance of having the right HT-CAC catalysts was even more pronounced at higher flow rates (200 ml/min, $W/F_{total} = 1 \times 10^{-3}$ (g·min)/ml). In these cases, bare support, sand, or an empty tube resulted in significant NH_3 slip, with NH_3 conversions below 90% at 1100°C. In contrast, 0.5Pt/10ZrAl maintained 100% NH_3 conversion, with NO_x emissions under 40 ppm. The T_{10} values dropped to approximately 200°C.

Understanding the 10%ZrO_2-Al_2O_3 support material

Various characterisation techniques were applied to study the 0.5Pt/10ZrAl catalyst and related materials to gain insights into how they facilitate the HT-CAC process. The initial focus was on understanding the properties of the support material. Aluminium oxides (Al_2O_3), particularly γ-Al_2O_3, are commonly employed as the catalyst support due to their large surface areas and good thermal stability. However, at temperatures between 700 to 800℃, γ-Al_2O_3 will be converted to δ-Al_2O_3 and θ-Al_2O_3, eventually forming α-Al_2O_3 at temperatures around 1000℃.[46] This phase transformation usually results in sintering and a reduction in specific surface areas.[47] In this work, the Al_2O_3 was prepared by calcining AlN precursors (see the Method section). X-ray Diffraction (XRD) experiments show that the resulting Al_2O_3, indeed, predominantly contains the α-Al_2O_3 phase after being calcined at 1100°C in the air for 4 hours (**Figure S5A**), resulting in a significant reduction in the BET-specific surface area (**Figure S5B**).

A common strategy for maintaining higher surface area in Al_2O_3 is incorporating dopants or additives to inhibit phase transitions.[48] ZrO_2 was reported [49,50] as an effective additive for this purpose. We found that by adding 10wt% ZrO_2 into the synthesis process of Al_2O_3, the resulting material (denoted as 10ZrAl) provided the highest BET surface area at 1100°C (about 67 m^2/g) among other compositions we have tried (*i.e.*, 2.5 wt%, 5 wt% or 20 wt% of ZrO_2). XRD results confirmed that a significant amount of θ-Al_2O_3 co-exists with the α-Al_2O_3 in the 10ZrAl after the same calcination heat treatment at 1100°C (**Figure S5A**). The BET surface area of the 10ZrAl after calcined at 1100°C in air for 4 hours was about 67 m^2/g (**Figure S5B**), which is higher compared to pure Al_2O_3 (< 40 m^2/g) or pure ZrO_2 (~10 m^2/g, **Figure S6**) prepared in similar approaches. In addition, 10ZrAl gave identical hysteresis loops and the Type IV N_2 adsorption isotherms[51] (**Figure S7**) compared to Al_2O_3, indicating that adding ZrO_2 does not significantly affect the pore distributions of Al_2O_3.

Representative scanning transmission electron microscopy (STEM) high-angle annular dark field (HAADF) images of the fresh and used 10ZrAl are shown in **Figure S8**. The support consists of a mixture of Al_2O_3 and ZrO_2 particles, approximately 10-20 nm in size. Atomically dispersed species with higher contrast are observed on both ZrO_2 and Al_2O_3 particles in both fresh and used materials, potentially originating from Hf impurities in the ZrO_2 precursors or Zr doping in Al_2O_3 (**Table S3**). The catalytic performance of 10ZrAl, Al_2O_3, and ZrO_2 in HT-CAC is summarized in **Table S1** (**entries 4, 6, 8,** and **9**). Among these, 10ZrAl demonstrated the highest N_2 selectivity and the lowest NO_x emissions (<40 ppm) at high temperatures, outperforming both Al_2O_3 and ZrO_2. However, the ignition

temperatures for 10ZrAl remained relatively high, with T_{10} around 470°C and T_{90} around 600°C.

Identify atomically dispersed Pt in the 0.5Pt/10ZrAl catalyst as active sites for HT-CAC.

As shown earlier, adding 0.5 wt% Pt onto the 10ZrAl support material using a one-pot synthesis method significantly improved the activities at both low-temperature and high-temperature regimes while maintaining high N_2 selectivity at 1100°C. The BET surface area of the resulted catalyst 0.5Pt/10ZrAl reduced after being used in the HT-CAC but stabilised at approximately 20 m^2/g (**Figure S9**). From XRD (**Figure S10)**, a significant amount of θ-Al_2O_3 phase was also found in 0.5Pt/10ZrAl materials, consistent with the case of the bare 10ZrAl support. Scanning electron microscopy (SEM) backscattered electron (BSE) images (**Figure S11**) of the fresh and used 0.5Pt/10ZrAl catalysts where Pt particles with sizes around tens or hundreds of nanometers are found. Despite this, atomically dispersed Pt species were identified in both fresh (**Figure S12**) and used catalysts (**Figures S13**, **S14**). To address the potential co-existence of atomically dispersed Hf or Zr, correlative electron microscopy imaging and XEDS analysis confirmed that at least some of the isolated atoms observed in HAADF images were atomically dispersed Pt species. Notably, even after 80 hours of HT-CAC reaction at 1100°C (8 consecutive 10-hour runs), atomically dispersed Pt species remained present in the 0.5Pt/10ZrAl-usedx1-80h material (**Figure S15**). This underscores the stability and critical role of atomically dispersed Pt as active sites in the HT-CAC process.

The presence of atomically dispersed Pt species can also detected via CO-DRIFTS spectroscopy. As shown in **Figure 3I**, the fresh catalyst contains both Pt nanoparticles as well as atomically dispersed Pt species. After being used, the peak corresponding to atomically dispersed Pt becomes more prominent. Pt L_3-edge X-ray Absorption Fine Structure (XAFS) spectroscopy studies were performed. While Pt particles dominate the Extended X-ray Absorption Fine Structure (EXAFS) results (**Figure S16, Table S4**) and the detection of Pt-Pt bonds were inevitable, a clear presence of Pt-O bonds was also observed. This is consistent with other direct evidence of atomically dispersed Pt species, such as CO-DRIFTS and electron microscopy results. The amount of atomically dispersed Pt species in the catalysts can be estimated using X-ray Absorption Near Edge Structure (XANES) through linear least squares fitting with reference spectra of metallic Pt foil and a previously reported single-atom catalyst, 0.2Pt/m-Al_2O_3-O_2[52] (**Figure S17**). The fitting results (**Figures 3J** and **S18**) revealed that ~45% of the Pt in the fresh 0.5Pt/10ZrAl catalyst was atomically dispersed. This fraction decreased to

approximately 20% in the 0.5Pt/10ZrAl-usedx1 catalyst. Additional usage in HT-CAC did not further change this fraction significantly, as about 22% of Pt in the 0.5Pt/10ZrAl-usedx1-10h catalyst were atomically dispersed. These results suggest that the quantity of atomically dispersed Pt stabilises after the first HT-CAC cycle, highlighting the durability of these atomically dispersed Pt sites during the process.

Integrating evidence from STEM, BET, CO-DRIFTS, and XAFS analyses, we conclude that the 0.5Pt/10ZrAl catalyst contains both atomically dispersed Pt species and relatively large Pt particles. No small nanoparticles were observed in the 0.5Pt/10ZrAl-usedx1 catalyst, these particles likely agglomerated significantly during HT-CAC at 1100°C. This extensive agglomeration makes them difficult to detect using high-resolution TEM and suggests that they contribute minimally to the surface area and catalytic activity. In other words, the activated 0.5Pt/10ZrAl catalyst can be considered a single-atom catalyst, despite having large Pt particles as spectators. The excellent catalytic activity towards ammonia (*i.e.*, $T_{90} < 250$°C), further suggests that the low-temperature regime is primarily due to the atomically dispersed Pt species. In the high-temperature regime, the improvement in N_2 selectivity observed after the HT-CAC cycle is likely associated with the agglomeration of Pt particles, as large Pt particles or bulk Pt are known to promote NO formation during processes such as the Ostwald process.[53]

To verify the hypothesis that atomically dispersed Pt species are the key active and selective sites in HT-CAC, we prepared several model catalysts. One such reference catalyst, 0.5Pt/Al_2O_3, was prepared using the same method as 0.5Pt/10ZrAl, except without adding Zr. Analysis of this catalyst revealed the presence of both atomically dispersed Pt species and small nanoparticles, as confirmed by *in situ* CO-DRIFTS spectra (**Figure S19**), STEM-HAADF images (**Figure S20**), and STEM-XEDS results (**Figure S21**). As shown in **Table S1** and **Figure S22**, the 0.5Pt/Al_2O_3 catalyst also exhibited an activation effect after the first HT-CAC run, consistent with the behaviour observed for the 0.5Pt/10ZrAl catalyst.

Next, we attempted to selectively remove metallic Pt species (*i.e.*, Pt particles) from the 0.5Pt/10ZrAl-usedx1 catalyst using a sodium cyanide (NaCN) leaching method.[62,63] are the primary active sites while Pt particles act as spectators, minimal changes in catalytic performance would be expected after leaching. This hypothesis was validated experimentally. After treatment with a 2 wt.% NaCN solution at 40°C for 6 hours, the resulting catalyst (0.5Pt/10ZrAl-usedx1-NaCN) exhibited a

reduction in Pt loading from 0.52 wt.% to ~0.4 wt.%, as measured by ICP-OES (**Table S5**). Despite this reduction, the leached catalyst maintained nearly identical low-temperature catalytic properties, including T_{10} and T_{90}, as compared to the original catalyst (**Table S1**, **Figures 4A**, **4B**, and **S23**). CO-DRIFTS and STEM imaging confirmed the presence of atomically dispersed Pt species after leaching (**Figures 4C-E** and **S24**). A temporary increase in NO_x emissions (~335 ppm) was observed at the zeroth hour mark for the leached catalyst, likely caused by the formation of small Pt particles, either due to redeposition or incomplete dissolution of larger particles during the leaching process. However, as the reaction progressed, these small particles likely agglomerated, reducing NO_x emissions to levels (~31 ppm) comparable to the unetched sample.

We also prepared another model catalyst, loading 0.5 wt% of Pt onto a pre-made 10ZrAl support using an incipient wet-impregnation (IWI) method. The resultant material, labelled as IWI-0.5Pt/10ZrAl, again exhibited a similar *in situ* activation behaviour to our best 0.5Pt/10ZrAl catalyst. As shown in **Figures 4F** and **S25**, for the 2nd run in HT-CAC using this model catalyst, the T_{90} was lowered from 435℃ to 265℃, and the N_2 selectivity increased from about 77% to about 85%. According to *in situ* CO-DRIFTS (**Figure 4G**), SEM-BSE (**Figure S26**), STEM-HAADF and XEDS results (**Figures 4F, 4I** and **S27**), the fresh IWI-0.5Pt/10ZrAl catalyst mainly contains small Pt nanoparticles with roughly 1-3 nm in size. However, after use in HT-CAC, atomically dispersed Pt species were identified along with some residual Pt nanoparticles. These findings reinforce the hypothesis that single-atom Pt sites are critical for achieving high catalytic activity (low ignition temperature), stability, and N_2 selectivity at 1100°C in HT-CAC. This consistency across different preparation methods highlights the pivotal role of atomically dispersed Pt species in optimizing HT-CAC performance.

Understanding the *in situ* activation effect of the 0.5Pt/10ZrAl catalyst for HT-CAC.

The fact that *in situ* activation phenomena were consistently observed after the first HT-CAC run for 0.5Pt/10ZrAl and other model catalysts presents an intriguing question: How can the high-temperature HT-CAC process, which causes severe sintering of Pt particles and thus reduces NO_x emission sites, simultaneously enhance low-temperature catalytic activities?

Earlier we showed that the fraction of atomically dispersed Pt species, as determined by XANES (**Figure 3L**), decreased from approximately 45% in the fresh 0.5Pt/10ZrAl catalyst to about 20% in

the 0.5Pt/10ZrAl-usedx1 catalyst. Since the catalyst was prepared via one-pot synthesis, some Pt species were likely trapped within the support, contributing to the XANES signal while remaining inaccessible for catalysis. To evaluate the evolution of surface-accessible Pt sites after HT-CAC, we conducted CO chemisorption experiments (**Figure 5A**). The total CO adsorption per gram of catalyst slightly decreased from ~197 μL/g for the fresh 0.5Pt/10ZrAl catalyst to ~188 μL/g for the used 0.5Pt/10ZrAl-usedx1 catalyst. Considering that both the support material[54] (**Figure S28**) and Pt contribute to CO chemisorption and that their surface areas differ significantly, we tested the bare support and normalized all CO chemisorption data by their corresponding BET surface areas (**Figure S9**). The results revealed that the used 0.5Pt/10ZrAl catalyst exhibited a significantly higher CO uptake (4.8 μL/ m^2) compared to the fresh catalyst (2.2 μL/m^2). This strongly suggests that new adsorption sites were created on the catalyst surface after the first HT-CAC run. According to CO-DRIFTS results (**Figure 3I**), these new sites are likely atomically dispersed Pt species. Subtracting the estimated contribution from the support, we found that the Pt dispersion increased from approximately 16% for the fresh catalyst to about 23% for the 0.5Pt/10ZrAl-usedx1 catalyst (**Table S6**).

A plausible explanation for this increase of atomically dispersed species on the surface during HT-CAC is schematically illustrated in **Figure 5B**. The fresh 0.5Pt/10ZrAl catalyst contains Pt nanoparticles (NPs) and atomically dispersed Pt species, with some of the latter being embedded within the support and inaccessible at the surface. During the first HT-CAC run, the high-temperature conditions likely cause Pt particles and some atomically dispersed Pt species to undergo sintering, forming larger particles. Concurrently, embedded Pt species may migrate to the surface, replenishing and possibly increasing the population of surface-accessible active Pt atoms. Additional HT-CAC runs did not further enhance low-temperature activity, likely because the catalyst structure stabilises after the first cycle and any available embedded Pt atoms are depleted. This aligns well with observations in co-precipitated catalysts, where embedded metal species migrate outward during high-temperature treatments.[55] Consistent with this picture, the total amount of atomically dispersed Pt species (~20%) in the 0.5Pt/10ZrAl-usedx1 catalyst, obtained from XANES, matches well with its Pt dispersion (~23%), estimated from CO chemisorption. This indicates that minimal embedded Pt species remain within the catalyst support after the first HT-CAC run. Another possible route for generating isolated Pt sites is the redispersion of Pt particles. At the high-reaction temperature, mobile Pt species could be trapped by surface defects on the support, thus creating additional atomically dispersed Pt species, as

previously reported.[56-58] This mechanism could also explain why similar *in situ* activation behaviour was observed for the impregnated sample (IWI-0.5Pt/10ZrAl), where the pre-formed support should not contain a significant amount of embedded Pt species.

The nature of the active sites on the fresh and used catalysts was investigated using O_2-TPD, with the results scaled according to the BET surface area of the fresh 0.5Pt/10ZrAl and 0.5Pt/10ZrAl-usedx1 catalysts (**Figure 5C**). Both catalysts exhibited similar O_2-TPD profiles,[59-61] with a peak around 230°C corresponding to surface chemisorbed oxygen and a broad peak around 450°C likely associated with adsorbed oxygen related to oxygen vacancies on the support. At the low-temperature regime where the *in situ* activation phenomenon was observed, the two catalysts displayed very similar oxygen activation capabilities.

NH_3-DRIFTS was also carried out to investigate the reaction mechanism at the low-temperature regime. Compared to the bare support 10ZrAl-usedx1, both fresh and used 0.5Pt/10ZrAl materials exhibited enhanced NH_3 absorption, evident in stronger IR bands corresponding to NH_3 on Lewis- and Bronsted-acid sites (**Figure S29**).[62-64] Fresh 0.5Pt/10ZrAl displayed stronger NH_3 absorption peaks, probably due to its higher surface area compared to 0.5Pt/10ZrAl-usedx1. O_2 was introduced at 220°C, close to the $T_{10,}$ for both fresh (236°C) and used (210°C) 0.5Pt/10ZrAl catalysts. As shown in **Figures 5D, 5E**, **S30** for fresh 0.5Pt/10ZrAl, NH_3 species on Lewis acid sites dropped after 30 mins indicating the oxidation reaction took place. New IR features[62-64] appeared on both catalysts, corresponding to intermediates such as -NH_2 (ca. 1349 cm^{-1} and 1556 cm^{-1}), -NH (ca. 1445 cm^{-1}), and -HNO (ca. 1520 cm^{-1} and 1882 cm^{-1}), consistent with the imide mechanism previously reported for NH_3 selective catalytic oxidation (NH_3-SCO) on Pt/Al_2O_3 and similar catalysts.[65] At T_{10} (~215°C) and 2 vol.% NH_3, the 0.5Pt/10ZrAl-usedx1 catalyst exhibited a reaction rate of ~$1.2 \cdot 10^7$ $ml_{NH3}mol_{Pt}^{-1}h^{-1}$. This is nearly identical to the previous study by Fudong Liu[66] and colleagues on Pt single atoms on Al_2O_3, where they recorded a rate of ~$2.0 \cdot 10^5$ $ml_{NH3}mol_{Pt}^{-1}h^{-1}$ at T_{10} (~210°C) with 0.05 vol.% NH_3 (500 ppm), considering NH_3 oxidation in dilute NH_3 and O_2 can be treated as a first-order reaction to the concentration of NH_3.[67]

In summary, these experimental results indicate that the *in situ* activation phenomenon is mainly associated with an increase in the number of accessible single-atom Pt sites on the surface. This also reinforces our previous argument that those single-atom Pt species are the active sites for HT-CAC. The behaviours of these single-atom Pt sites on the 10ZrAl support were found to be consistent

compared to previous reports.[66]

CONCLUSIONS AND PERSPECTIVES

This study demonstrated that the 0.5Pt/10ZrAl catalyst effectively facilitates the HT-CAC process at 1100°C. The catalyst successfully ignited a dilute (2% NH_3) and fuel-lean ($\lambda = 1.5$) NH_3-air mixture with a low ignition temperature of just above 200°C. At 1100°C, the catalyst exhibited excellent stability and effective NO_x emission control (~50 ppm) without detectable NH_3 slip, confirming the feasibility of HT-CAC as a challenging but achievable reaction.

Detailed characterizations and model catalyst investigations revealed that atomically dispersed Pt species are the active sites for HT-CAC. At low temperatures, these single-atom Pt sites follow the imide mechanism for NH_3 oxidation, behaving consistently with previous reports and achieving comparable reaction rates. At high temperatures, significant contributions from homogeneous reactions are expected, presenting challenges for a molecular-level understanding of catalytic contributions under extreme conditions. Novel tools and methodologies will likely be required to address these challenges.

From a practical standpoint, a NH_3-based energy infrastructure does not yet exist, and NH_3 is still produced as a chemical rather than a fuel. The cost of the NH_3 fuel and the equipment, as well as safety considerations, have limited the scale of the current study both in space and time. Nevertheless, the 0.5Pt/10ZrAl catalyst demonstrated good potential to be scaled up. The catalyst achieved 100% NH_3 conversion at W/F=$1x10^{-3}$ g min/ml, translating to a gas hourly space velocity (GHSV) of 11,000 h^{-1} in our packed-bed reactor. This is approaching the condition used in relevant processes that have already been scaled up. For instance, the commercial volatile organic compound (VOC) combustion catalyst usually contains 1-2 wt. % supported noble metal and was operated at dilute fuel concentration (*e.g.*, < 1 vol.% VOC) a GSHV around 10000-20000 h^{-1} in a monolithic reactor.[68]

Another example is the catalytic flow reversal reactors (FRR) that are used for heat recovery in ventilation air methane (VAM) combustion. Kucharczyk *et al.*[69] obtained the activity data of various palladium catalysts for VAM combustion in a large laboratory scale (20-30 m^3 h^{-1} gas flow with 0.4-0.9 vol. % CH_4) at first and then chose Pd/monolithic and Pd/Al_2O_3 catalysts for a medium-sized catalytic FRR (length: 2.1 m, inner diameter: 0.66 m) test. This catalytic FRR can be autothermal when ventilation air flow rate at 3000-3500 m^3 h^{-1} and 0.5-0.6 vol. % CH_4 (GHSV= 5850 h^{-1}). Gosiewski *et*

al.[70] later conducted the VAM combustion test in a medium-sized thermal FRR plant with a VAM flow rate of 400 m^3_{STP}/h, and the reaction reached about 1100℃, and the temperature of the withdrawn hot gas reached 950℃. The reaction is non-catalytic partially because no suitable high-temperature combustion catalyst was developed or identified. Drawing parallels between VAM combustion and HT-CAC, and leveraging the demonstrated high-temperature stability of the 0.5Pt/10ZrAl catalyst, we deduce that HT-CAC has strong potential for scale-up under autothermal conditions.

EXPERIMENTAL PROCEDURES

Materials synthesis

The synthesis of 10ZrAl (10%ZrO_2-Al_2O_3). Firstly, adding 2g aluminium nitride (AlN, Sigma Aldrich, CAS: 24304-00-5), 0.216g zirconyl nitrate ($ZrO(NO_3)_2 \cdot xH_2O$, Sigma Aldrich, CAS: 14985-18-3) and 40ml deionised water into the beaker, then stirred at room temperature for one hour and heated to 80℃ until getting the dry mixture. Secondary, calcining the collected sample to 550℃ by 5℃/min (BEQ, BTF-1200C-S) for 30min in air to get 10%ZrO_x-AlO_y oxides. Finally, calcining 10%ZrO_x-AlO_y at 1000℃ (BEQ, BTF-1200C-S) by 5℃/min for 4 hours in air to get a fresh 10%ZrO_2-Al_2O_3 product.

The synthesis of Al_2O_3. The Al_2O_3 support material was prepared by directly calcining AlN in air. Initially, the AlN was calcined at 550°C for 30 minutes, followed by cooling to room temperature. Subsequently, the samples were further calcined at 1000°C using a heating rate of 5°C/min and held at this temperature for four hours in air.

The synthesis of ZrO_2. The ZrO_2 material was prepared by directly calcining $ZrO(NO_3)_2 \cdot xH_2O$ in air. Initially, the precursor was calcined at 550°C for 30 minutes, followed by cooling to room temperature. The samples were then calcined at 1000°C using a heating rate of 5°C/min and held at this temperature for four hours in air.

The synthesis of 0.5Pt/10ZrAl (0.5%Pt/10%ZrO_2-Al_2O_3) by one-pot way. Firstly, adding 2g AlN, 0.216g $ZrO(NO_3)_2 \cdot xH_2O$, 0.5 wt. % Pt ($H_2PtCl_6 \cdot 6H_2O$, Sigma Aldrich, CAS: 18497-13-7) and 40ml deionised water into the beaker, then stirred at room temperature for one hour and heated to 80℃ until

getting the dry mixture. Secondary, calcining the collected sample to 550℃ by 5℃/min for 30min in air to get 0.5%Pt/10%ZrO_x-AlO_y oxides. Finally, calcining 10%ZrO_x-AlO_y at 1000℃ by 5℃/min for 4h in air to get fresh 0.5Pt/10ZrAl product.

The synthesis of model catalyst of IWI-0.5Pt/10ZrAl. Directly adding 0.5 wt. % Pt ($H_2PtCl_6 \cdot 6H_2O$) according to the mass of as-prepared 10%ZrO_2-Al_2O_3 powder, and then stirring at room temperature for 1h and heated to 80℃ until getting the dry mixture. This is followed by calcining 10%ZrO_x-AlO_y at 400℃ by 5℃/min for two hours in air to get fresh IWI-0.5Pt/10ZrAl catalyst.

The NaCN etching treatment. Adding a certain amount of sodium cyanide (NaCN, 2 wt.%) to NaOH solution with a pH of 12, then adding the sample. Heating while stirring to 40℃ and maintaining for 6 hours. Washing the sample with NaOH solution and deionised water for several times by centrifugation, and finally drying at 80℃ overnight.

The HT-CAC reaction tests

The catalytic performance evaluation system shown in **Figure S1** mainly includes the high temperature furnace (GSL-1700X-VTφ60), calibrated mass flowrate controller (MFC, Sevenstar, D07-7D), and the mass spectrometer (MS, Hidden Analytical, HPR-20 R&D), using a 7 mm inner and 12 mm outer diameter corundum tube. The MS was used to detect the gas concentration before and after the reaction. Before the NH_3 catalytic combustion reaction, 200 mg catalysts and about 1000 mg quartz sand (50-70 mesh, Sigma Aldrich) were mixed evenly and then put into the quartz tube. The temperature rising rate during reaction is fixed at 10℃/min, and the furnace is kept at constant temperature for 10 minutes at 200, 300, 500, 700, 900, 1100℃, respectively.

Test condition 1: 2 vol.% NH_3 (Air liquid, 99.9995%), 3 vol.% O_2 by 10%O_2/Ar (Air liquid, >99.9%), while using pure Ar (Air liquid) as the balance gas. **The total gas flow rate was 100 mL min^{-1} to meet a W/F_{total} of $2x10^{-3}$ g min_{ml}^{-1}, GHSV = 5500 h^{-1}.** Note: GHSV in this work was calculated by the total flowrate divides the volume of catalysts bed (about 1.1ml), including the catalyst and sand. In this condition, the NH_3 conversion (λ) was calculated at the temperature range of 200-1100 °C, which was calculated by Eq. (1):

$$\lambda=(C_{in}-C_{out})/C_{in} *100\% \quad (1)$$

where C_{in} and C_{out} refer to the NH_3 concentration of the inlet and outlet, respectively.

The final N_2 selectivity is calculated by Eq. (2):

$$N_2 \text{ selectivity} = C_{N2}/(C_{N2}+C_{NO}+C_{N2O}) *100\% \quad (2)$$

C is the concentration of the gas in the total flow.

While the final NO_x emissions (ppm) are calculated by Eq. (3):

$$NO_x \text{ emissions}= (C_{NO}+C_{N2O})/(C_{N2}+C_{NO}+C_{N2O}+C_{Ar}+C_{O2}+C_{NH3}+C_{H2O}) \quad (3)$$

Test condition 2: 2 vol.% NH_3 (Leeden NO_x, 99.9995%), 3 vol.% O_2 by compressed air (Air liquid), while using pure N_2 (Air liquid) as the balance gas. The total gas flow rate was **100 mL min^{-1} to meet a W/F$_{total}$ of 2x10^{-3} g min$_{ml}^{-1}$, GHSV = 5500 h^{-1}.**

Test condition 3: 2 vol.% NH_3 (Leeden NO_x, 99.9995%), 3 vol.% O_2 by compressed air (Air liquid), while using pure N_2 (Air liquid) as the balance gas. The total gas flow rate was **200 mL min^{-1} to meet a W/F$_{total}$ of 1x10^{-3} g min$_{ml}^{-1}$, GHSV = 11000 h^{-1}.**

The NH_3 conversion (λ) was calculated at the temperature range of 200-1100°C, which was calculated by Eq. (4):

$$\lambda=(C_{in}-C_{out})/C_{in} \text{ x}100\% \quad (4)$$

where C_{in} and C_{out} refer to the NH_3 concentration of the inlet and outlet, respectively.

In this case, because the N_2 is the balance gas (~95 vol. % N_2 in total) for the reaction, while the N_2 also is the production from the HT-CAC reaction, thus the accurate N_2 selectivity in test conditions 2 and 3 were hard to get.

While the final NO_x emissions (ppm) are calculated by Eq. (5):

$$NO_x \text{ emissions}= (C_{NO}+C_{N2O})/(C_{N2}+C_{NO}+C_{N2O}+C_{Ar}+C_{O2}+C_{NH3}+C_{H2O}) \quad (5)$$

Catalyst Characterizations

The crystal structure was investigated using X-ray diffraction (XRD) with a Bruker D8 advance instrument. The range of 2θ was from 10° to 90°.

The element content was analyzed using inductively coupled plasma optical emission spectroscopy

(ICP-OES) with a Perkin Elmer Avio 500 instrument. Solid samples were digested with a mixture of HCl, HNO_3 and HF.

The surface morphology of the 10%ZrO_2-Al_2O_3 and Al_2O_3 samples was characterized using scanning electron microscopy (SEM) with a Zeiss Sigma 300 instrument.

The morphology and elemental mapping of these catalysts were investigated using aberration-corrected scanning transmission electron microscopy (AC-STEM). This was conducted on a JEOL ARM 200CF operating at 200 kV at the National University of Singapore, which is equipped with Oxford Instruments X-ray energy-dispersive spectrometer, and a Thermo Fisher Themis Z operating at 300 kV at East China University of Science and Technology, equipped with four in-column Super-X detectors. To confirm the existence of Pt atoms within these catalysts, transmission electron microscopy (TEM) bright field (BF) imaging, STEM high-angle annular dark-field (HAADF) imaging, and corresponding X-ray energy-dispersive spectroscopy (X-EDS) analysis were performed using a JEOL JEM-2800 microscope operating at 200 kV. This microscope is equipped with a JEOL EDS detection system featuring 100 mm^2 Silicon Drift Detectors (SDDs) with a collection angle of approximately 0.95 steradians. Gaussian peak fitting was employed to differentiate between the Pt L and Au L peaks, while the background intensity was determined through linear fitting.

The BET specific surface areas and N_2 adsorption isotherms were determined using a Micromeritics 3 Flex adsorption analyzer after degassing the sample for 12 hours at 200°C in N_2.

The *in situ* CO-DRIFTS was conducted using a Nicolep iS50 instrument. The sample was reduced at 300°C for 60 minutes by 5 vol.% H_2/N_2 at first, and then cooled down to 30°C to obtain the background spectrum in Ar. Following the spectrum was collected when the 5 vol.% CO/N_2 was opened, finally changed to Ar after adsorption CO for 15min. All the spectra were recorded by accumulating 64 scans at a resolution of 4 cm^{-1}.

The X-ray Absorption Fine Structure (XAFS) study was carried out at the Singapore Synchrotron Light Source (SSLS). Spectra were collected at the Pt L_3 edge (11564 eV). Data were collected in the

transmission mode. In a typical experiment, about 150 mg of catalysts were pelletized. Several scans were acquired to increase the signal-to-noise ratio and ensure reproducibility of data. Pt foil and PtO_2 were used as references. Data analysis was done on Athena and Artemis software developed by B. Ravel and M. Newville.[71] After appropriate background subtraction, data ranges were assessed based on the quality of data generally for k = 1.6-12.4 $Å^{-1}$ and for R = 1.7-3.2 Å. The fitting results are given in Table S4.

The CO titration for Pt dispersions using an Autosorb IQ-C-AG (1 Stat.) EPDM instrument. The sample was reduced at 300°C for 60 minutes by 5 vol.% H_2/N_2 at first, and then cooled down to 50°C to start CO titration procedures (27.7 µL per cycles, 6-10 cycles to saturate).

The O_2 temperature-programmed desorption (O_2-TPD) experiments were conducted using an Autosorb IQ-C-AG (1 Stat.) EPDM instrument. Each sample was pretreated at 350°C for 60 minutes under a helium atmosphere to remove impurities, then cooled to 50°C. Subsequently, 10% O_2 was adsorbed onto the sample for 30 minutes. Following a 60-minute helium purge to eliminate any unadsorbed species, the final measurements were recorded over a temperature range of 50 to 800°C, with a heating rate of 10°C/min.

The *in situ* NH_3-DRIFTS at 220°C was conducted using a Nicolep iS50 instrument. The sample was treated at 300°C for 60 minutes by 20ml/min Ar to remove surface impurities at first, and then cooled down to 220°C to obtain the background spectrum in Ar. Following the 2 vol.% NH_3/Ar (100ml/min) flowed into the sample holder for 30min and changed to 20ml/min Ar for another 30min. Finally, the 3 vol.% O_2/Ar (100ml/min) was introduced to get the final data at 220°C for 30min. All the spectra were recorded by accumulating 64 scans at a resolution of 4 cm^{-1}.

SUPPLEMENTAL INFORMATION

Please see in *Supplementary Information*.

ACKNOWLEDGMENTS

We acknowledge the support by National Research Foundation (NRF) Singapore, under its NRF

Fellowship (NRF-NRFF11-2019-0002). We also thank the Singapore Low-Carbon Energy Research Funding Initiative hosted under A*Star for the financial support (Award No. U2102d2005; U2102d2006; U2305d4003). We thank the approval of JASRI (proposal no. 2023A1533) to use beamline BL01B1, SPring-8 (Japan Synchrotron Radiation Research Institute, Hyogo, Japan) for XAS measurements.

AUTHOR CONTRIBUTIONS

Q.H. conceived the project. Y.D., co-supervised by Q.H. and N.Y., conducted most experiments including synthesis, characterization, and testing, as well as data analysis. B.Y., supervised by Q.H. carried out STEM characterization of the catalysts under the supervision of S.D. and prepared the relevant part of the manuscript. L. X. assisted in experimental tests. S. L., C. X., S. W., and S.X. participated in the material characterizations. P. H. assisted in the data analysis. Y.D. and Q.H. drafted the paper. N.Y. revised the paper. All authors discussed the paper.

DECLARATION OF INTERESTS

The authors declare no competing interests.

REFERENCES

1. Woodall, C.M., Fan, Z., Lou, Y., Bhardwaj, A., Khatri, A., Agrawal, M., McCormick, C.F., and Friedmann, S.J. (2022). Technology options and policy design to facilitate decarbonization of chemical manufacturing. Joule *6*, 2474-2499. 10.1016/j.joule.2022.10.006.
2. Krishnan, M., Samandari, H., Woetzel, J., Smit, S., Pacthod, D., Pinner, D., Nauclér, T., Tai, H., Farr, A., Wu, W., and Imperato, D. (2022). Sectors are unevenly exposed in the net-zero transition.
3. Fan, Z., and Friedmann, S.J. (2021). Low-carbon production of iron and steel: Technology options, economic assessment, and policy. Joule *5*, 829-862. 10.1016/j.joule.2021.02.018.
4. Sutherland, B.R. (2020). Sustainably Heating Heavy Industry. Joule *4*, 14-16. 10.1016/j.joule.2019.12.020.
5. Sandalow, D., Friedmann, J., Aines, R., McCormick, C., and others (2019). ICEF Industrial heat decarbonization roadmap. Innovation for Cool Earth.
6. Mallapragada, D.S., Dvorkin, Y., Modestino, M.A., Esposito, D.V., Smith, W.A., Hodge, B.-M., Harold, M.P., Donnelly, V.M., Nuz, A., Bloomquist, C., et al. (2023). Decarbonization of the chemical industry through electrification: Barriers and opportunities. Joule *7*, 23-41. 10.1016/j.joule.2022.12.008.
7. Thiel, G.P., and Stark, A.K. (2021). To decarbonize industry, we must decarbonize heat. Joule

5, 531-550. 10.1016/j.joule.2020.12.007.

8. Elishav, O., Mosevitzky Lis, B., Miller, E.M., Arent, D.J., Valera-Medina, A., Grinberg Dana, A., Shter, G.E., and Grader, G.S. (2020). Progress and Prospective of Nitrogen-Based Alternative Fuels. Chem Rev *120*, 5352-5436. 10.1021/acs.chemrev.9b00538.
9. MacFarlane, D.R., Cherepanov, P.V., Choi, J., Suryanto, B.H.R., Hodgetts, R.Y., Bakker, J.M., Ferrero Vallana, F.M., and Simonov, A.N. (2020). A Roadmap to the Ammonia Economy. Joule *4*, 1186-1205. 10.1016/j.joule.2020.04.004.
10. Smith, C., Hill, A.K., and Torrente-Murciano, L. (2020). Current and future role of Haber–Bosch ammonia in a carbon-free energy landscape. Energy & Environmental Science *13*, 331-344.
11. Wang, L., Xia, M., Wang, H., Huang, K., Qian, C., Maravelias, C.T., and Ozin, G.A. (2018). Greening Ammonia toward the Solar Ammonia Refinery. Joule *2*, 1055-1074. 10.1016/j.joule.2018.04.017.
12. Crolius, S.H. Great Strides in NH_3 Commitment and Progress in Australia – Ammonia Energy Association. https://www.ammoniaenergy.org/articles/great-strides-in-nh3-commitment-and-progress-in-australia/.
13. Gu, J., Hsu, C.-S., Bai, L., Chen, H.M., and Hu, X. (2019). Atomically dispersed Fe^{3+} sites catalyze efficient CO_2 electroreduction to CO. SCIENCE *364*, 1091-1094.
14. Japan aims to boost ammonia fuel demand to 3 mln tonnes a year by 2030. (2021). Reuters, 2021/2/8. https://www.reuters.com/article/japan-energy-ammonia-idUSL4N2KE2HE.
15. Bal'zhinimaev, B.S., Paukshtis, E.A., Toktarev, A.V., Kovalyov, E.V., Yaranova, M.A., Smirnov, A.E., and Stompel, S. (2019). Effect of water on toluene adsorption over high silica zeolites. MICROPOROUS AND MESOPOROUS MATERIALS *277*, 70-77. 10.1016/j.micromeso.2018.10.023.
16. Yapicioglu, A., and Dincer, I. (2019). A review on clean ammonia as a potential fuel for power generators. Renewable and Sustainable Energy Reviews *103*, 96-108. 10.1016/j.rser.2018.12.023.
17. Cardoso, J.S., Silva, V., Rocha, R.C., Hall, M.J., Costa, M., and Eusébio, D. (2021). Ammonia as an energy vector: Current and future prospects for low-carbon fuel applications in internal combustion engines. Journal of Cleaner Production *296*. 10.1016/j.jclepro.2021.126562.
18. Valera-Medina, A., Amer-Hatem, F., Azad, A.K., Dedoussi, I.C., de Joannon, M., Fernandes, R.X., Glarborg, P., Hashemi, H., He, X., Mashruk, S., et al. (2021). Review on Ammonia as a Potential Fuel: From Synthesis to Economics. Energy & Fuels *35*, 6964-7029. 10.1021/acs.energyfuels.0c03685.
19. Dimitriou, P., and Javaid, R. (2020). A review of ammonia as a compression ignition engine fuel. International Journal of Hydrogen Energy *45*, 7098-7118. 10.1016/j.ijhydene.2019.12.209.
20. Makhloufi, C., and Kezibri, N. (2021). Large-scale decomposition of green ammonia for pure hydrogen production. International Journal of Hydrogen Energy *46*, 34777-34787. 10.1016/j.ijhydene.2021.07.188.
21. Dolan, R.H., Anderson, J.E., and Wallington, T.J. (2021). Outlook for ammonia as a sustainable transportation fuel. Sustainable Energy & Fuels *5*, 4830-4841. 10.1039/d1se00979f.
22. Gao, F., Liu, Y., Sani, Z., Tang, X., Yi, H., Zhao, S., Yu, Q., and Zhou, Y. (2021). Advances in selective catalytic oxidation of ammonia (NH_3–SCO) to dinitrogen in excess oxygen: A review on typical catalysts, catalytic performances and reaction mechanisms. Journal of

Environmental Chemical Engineering *9*. 10.1016/j.jece.2020.104575.

23. Lan, T., Zhao, Y., Deng, J., Zhang, J., Shi, L., and Zhang, D. (2020). Selective catalytic oxidation of NH_3 over noble metal-based catalysts: state of the art and future prospects. Catalysis Science & Technology *10*, 5792-5810. 10.1039/d0cy01137a.
24. Jabłońska, M., and Palkovits, R. (2016). Copper based catalysts for the selective ammonia oxidation into nitrogen and water vapour—Recent trends and open challenges. Applied Catalysis B: Environmental *181*, 332-351. 10.1016/j.apcatb.2015.07.017.
25. Bartholomew, C.H., and Farrauto, R.J. (2005). Fundamentals of Industrial Catalytic Processes, 2nd Edition (John Wiley & Sons). 10.1002/9780471730071.
26. Chmielarz, L., and Jabłońska, M. (2015). Advances in selective catalytic oxidation of ammonia to dinitrogen: a review. RSC Advances *5*, 43408-43431. 10.1039/c5ra03218k.
27. Wang, C., Ren, D., Harle, G., Qin, Q., Guo, L., Zheng, T., Yin, X., Du, J., and Zhao, Y. (2021). Ammonia removal in selective catalytic oxidation: Influence of catalyst structure on the nitrogen selectivity. JOURNAL OF HAZARDOUS MATERIALS *416*. 10.1016/j.jhazmat.2021.125782.
28. Lietti, L., Groppi, G., and Ramella, C. (1998). NH3 oxidation during the catalytic combustion of biomasses-related fuels over Mn-substituted hexaaluminates. Catal. Letters *53*, 91-95. 10.1023/A:1019001821547.
29. Lietti, L., Cristiani, C., Groppi, G., and Forzatti, P. (2000). Preparation, characterization and reactivity of Me-hexaaluminate (Me=Mn, Co, Fe, Ni, Cr) catalysts in the catalytic combustion of NH_3-containing gasified biomasses. Catal. Today *59*, 191-204. 10.1016/S0920-5861(00)00283-2.
30. Burch, R., and Southward, B.W.L. (2001). The Nature of the Active Metal Surface of Catalysts for the Clean Combustion of Biogas Containing Ammonia. J. Catal. *198*, 286-295. 10.1006/jcat.2000.3131.
31. Berg, M., Magnus Johansson, E., and Järås, S.G. (2000). Catalytic combustion of low heating value gas mixtures: comparison between laboratory and pilot scale tests. Catal. Today *59*, 117-130. 10.1016/S0920-5861(00)00277-7.
32. Darvell, L.I., Heiskanen, K., Jones, J.M., Ross, A.B., Simell, P., and Williams, A. (2003). An investigation of alumina-supported catalysts for the selective catalytic oxidation of ammonia in biomass gasification. Catal. Today *81*, 681-692. 10.1016/S0920-5861(03)00166-4.
33. Hinokuma, S., Matsuki, S., Kawabata, Y., Shimanoe, H., Kiritoshi, S., and Machida, M. (2016). Copper Oxides Supported on Aluminum Oxide Borates for Catalytic Ammonia Combustion. The Journal of Physical Chemistry C *120*, 24734-24742. 10.1021/acs.jpcc.6b07157.
34. Hinokuma, S., Shimanoe, H., Matsuki, S., Kawano, M., Kawabata, Y., and Machida, M. (2016). Catalytic Activity and Selectivities of Metal Oxides and Pt/Al_2O_3 for NH_3 Combustion. Chemistry Letters *45*, 179-181. 10.1246/cl.151031.
35. Hinokuma, S., Kawabata, Y., Kiritoshi, S., Matsuki, S., and Machida, M. (2017). Operando XAFS studies of supported copper oxides for catalytic ammonia combustion. Journal of the Ceramic Society of Japan *125*, 770-772. 10.2109/jcersj2.17075.
36. Hinokuma, S., Kawabata, Y., Matsuki, S., Shimanoe, H., Kiritoshi, S., and Machida, M. (2017). Local Structures and Catalytic Ammonia Combustion Properties of Copper Oxides and Silver Supported on Aluminum Oxides. The Journal of Physical Chemistry C *121*, 4188-4196. 10.1021/acs.jpcc.6b13024.

37. Hinokuma, S., Kawabata, Y., Kiritoshi, S., Matsuki, S., and Machida, M. (2017). Operando XAFS studies of supported copper oxides for catalytic ammonia combustion. J. Ceram. Soc. Jpn. *125*, 770-772. 10.2109/jcersj2.17075.
38. Kiritoshi, S., Iwasa, T., Araki, K., Kawabata, Y., Taketsugu, T., Hinokuma, S., and Machida, M. (2018). Supported binary $CuO_{(x)}$ -Pt catalysts with high activity and thermal stability for the combustion of $NH_{(3)}$ as a carbon-free energy source. RSC Adv *8*, 41491-41498. 10.1039/c8ra07969b.
39. Hinokuma, S., Shimanoe, H., Kawabata, Y., Matsuki, S., Kiritoshi, S., and Machida, M. (2018). Effects of support materials and silver loading on catalytic ammonia combustion properties. Catalysis Today *303*, 2-7. 10.1016/j.cattod.2017.08.010.
40. Hinokuma, S., Shimanoe, H., Kawabata, Y., Kiritoshi, S., Araki, K., and Machida, M. (2018). Supported and unsupported manganese oxides for catalytic ammonia combustion. Catalysis Communications *105*, 48-51. 10.1016/j.catcom.2017.11.009.
41. Hinokuma, S., Araki, K., Iwasa, T., Kiritoshi, S., Kawabata, Y., Taketsugu, T., and Machida, M. (2019). Ammonia-rich combustion and ammonia combustive decomposition properties of various supported catalysts. Catalysis Communications *123*, 64-68.
42. Baukal, C. (2005). Everything you need to know about NO_x. Metal finishing *103*, 18-24.
43. Hou, Z., Lu, Y., Liu, Y., Liu, N., Hu, J., Wei, L., Li, Z., Tian, X., Gao, R., Yu, X., et al. (2023). A General Dual-Metal Nanocrystal Dissociation Strategy to Generate Robust High-Temperature-Stable Alumina-Supported Single-Atom Catalysts. Journal of the American Chemical Society *145*, 15869-15878. 10.1021/jacs.3c02909.
44. Lang, R., Du, X., Huang, Y., Jiang, X., Zhang, Q., Guo, Y., Liu, K., Qiao, B., Wang, A., and Zhang, T. (2020). Single-Atom Catalysts Based on the Metal–Oxide Interaction. CHEMICAL REVIEWS *120*, 11986-12043. 10.1021/acs.chemrev.0c00797.
45. Hannagan, R.T., Giannakakis, G., Flytzani-Stephanopoulos, M., and Sykes, E.C.H. (2020). Single-Atom Alloy Catalysis. CHEMICAL REVIEWS *120*, 12044-12088. 10.1021/acs.chemrev.0c00078.
46. Kovarik, L., Bowden, M., Andersen, A., Jaegers, N.R., Washton, N., and Szanyi, J. (2020). Quantification of High-Temperature Transition Al_2O_3 and Their Phase Transformations. Angewandte Chemie *132*, 21903-21911. 10.1002/ange.202009520.
47. Matori, K., Wah, L., Hashim, M., Ismail, I., and Zaid, M. (2012). Phase Transformations of α-Alumina Made from Waste Aluminum via a Precipitation Technique. International Journal of Molecular Sciences *13*, 16812-16821. 10.3390/ijms131216812.
48. Torrez-Herrera, J.J., Korili, S.A., and Gil, A. (2020). Progress in the synthesis and applications of hexaaluminate-based catalysts. Catalysis Reviews *64*, 592-630. 10.1080/01614940.2020.1831756.
49. Ipek, M., Zeytin, S., and Bindal, C. (2010). Effect of ZrO_2 on phase transformation of Al_2O_3. Ceramics International *36*, 1159-1163. 10.1016/j.ceramint.2009.12.017.
50. Boullosa-Eiras, S., Vanhaecke, E., Zhao, T., Chen, D., and Holmen, A. (2011). Raman spectroscopy and X-ray diffraction study of the phase transformation of ZrO_2–Al_2O_3 and CeO_2–Al_2O_3 nanocomposites. Catalysis Today *166*, 10-17. 10.1016/j.cattod.2010.05.038.
51. Cui, X., Chen, L., Wang, Y., Chen, H., Zhao, W., Li, Y., and Shi, J. (2014). Fabrication of Hierarchically Porous RuO_2–CuO/Al–ZrO_2 Composite as Highly Efficient Catalyst for Ammonia-Selective Catalytic Oxidation. ACS Catalysis *4*, 2195-2206. 10.1021/cs500421x.

52. Zhang, Z., Zhu, Y., Asakura, H., Zhang, B., Zhang, J., Zhou, M., Han, Y., Tanaka, T., Wang, A., Zhang, T., and Yan, N. (2017). Thermally stable single atom Pt/m-Al_2O_3 for selective hydrogenation and CO oxidation. Nature Communications *8*, 16100. 10.1038/ncomms16100.
53. Grande, C.A., Andreassen, K.A., Cavka, J.H., Waller, D., Lorentsen, O.-A., Øien, H., Zander, H.-J., Poulston, S., García, S., and Modeshia, D. (2018). Process Intensification in Nitric Acid Plants by Catalytic Oxidation of Nitric Oxide. Ind. Eng. Chem. Res. *57*, 10180-10186. 10.1021/acs.iecr.8b01483.
54. Pokrovski, K., Jung, K.T., and Bell, A.T. (2001). Investigation of CO and CO_2 adsorption on tetragonal and monoclinic Zirconia. Langmuir *17*, 4297-4303. 10.1021/la001723z.
55. Allard, L.F., Borisevich, A., Deng, W., Si, R., Flytzani-Stephanopoulos, M., and Overbury, S.H. (2009). Evolution of gold structure during thermal treatment of Au/FeO_x catalysts revealed by aberration-corrected electron microscopy. J. Electron Microsc. *58*, 199-212. 10.1093/jmicro/dfp016.
56. Rickard, J. (1990). Redispersion of platinum on Pt/Al_2O_3 model catalyst in oxygen studied by transmission electron microscopy. J. Catal. *121*, 141-152. 10.1016/0021-9517(90)90224-8.
57. Jones, J., Xiong, H., DeLaRiva, A.T., Peterson, E.J., Pham, H., Challa, S.R., Qi, G., Oh, S., Wiebenga, M.H., Pereira Hernández, X.I., et al. (2016). Thermally stable single-atom platinum-on-ceria catalysts via atom trapping. Science *353*, 150-154. 10.1126/science.aaf8800.
58. Tang, Z., Liu, P., Cao, H., Bals, S., Heeres, H.J., and Pescarmona, P.P. (2019). Pt/ZrO_2 Prepared by Atomic Trapping: An Efficient Catalyst for the Conversion of Glycerol to Lactic Acid with Concomitant Transfer Hydrogenation of Cyclohexene. ACS Catal. *9*, 9953-9963. 10.1021/acscatal.9b02139.
59. Fortunato, M.A., Princivalle, A., Capdeillayre, C., Petigny, N., Tardivat, C., Guizard, C., Tsampas, M.N., Sapountzi, F.M., and Vernoux, P. (2014). Role of lattice oxygen in the propane combustion over pt/yttria-stabilized Zirconia : Isotopic studies. Top. Catal. *57*, 1277-1286. 10.1007/s11244-014-0293-5.
60. Sun, M., Liu, J., Song, C., Ogata, Y., Rao, H., Zhao, X., Xu, H., and Chen, Y. (2019). Different Reaction Mechanisms of Ammonia Oxidation Reaction on Pt/$Al_{(2)}O_{(3)}$ and Pt/$CeZrO_{(2)}$ with Various Pt States. ACS Appl Mater Interfaces *11*, 23102-23111. 10.1021/acsami.9b02128.
61. Tian, Y., Han, Z., Li, Y., Zhao, H., Zeng, Q., and Cheng, S. (2024). Pt/Al_2O_3@Ce/ZrO_2-S bifunctional catalysts prepared by mechanically milling for selective catalytic oxidation of high-concentration ammonia. Environ. Sci. Pollut. Res. Int. *31*, 37746-37756. 10.1007/s11356-024-33744-6.
62. Amores, J.G., Escribano, V.S., Ramis, G., and Busca, G. (1997). An FT-IR study of ammonia adsorption and oxidation over anatase-supported metal oxides. Appl. Catal. B *13*, 45-58. 10.1016/s0926-3373(96)00092-6.
63. Ramis, G., Yi, L., and Busca, G. (1996). Ammonia activation over catalysts for the selective catalytic reduction of NO_x and the selective catalytic oxidation of NH_3. An FT-IR study. Catal. Today *28*, 373-380. 10.1016/s0920-5861(96)00050-8.
64. Ramis, G., Yi, L., Busca, G., Turco, M., Kotur, E., and Willey, R.J. (1995). Adsorption, activation, and oxidation of ammonia over SCR catalysts. J. Catal. *157*, 523-535. 10.1006/jcat.1995.1316.
65. Lan, T., Zhao, Y., Deng, J., Zhang, J., Shi, L., and Zhang, D. (2020). Selective catalytic oxidation of NH3over noble metal-based catalysts: state of the art and future prospects.

Catalysis Science & Technology *10*, 5792-5810. 10.1039/d0cy01137a.

66. Tan, W., Xie, S., Zhang, X., Ye, K., Almousawi, M., Kim, D., Yu, H., Cai, Y., Xi, H., Ma, L., et al. (2024). Fine-Tuning of Pt Dispersion on $Al_{(2)}O_{(3)}$ and Understanding the Nature of Active Pt Sites for Efficient CO and $NH_{(3)}$ Oxidation Reactions. ACS Appl Mater Interfaces *16*, 454-466. 10.1021/acsami.3c11897.
67. Long, R.Q., and Yang, R.T. (2001). Selective catalytic oxidation (SCO) of ammonia to nitrogen over Fe-exchanged zeolites. J. Catal. *201*, 145-152. 10.1006/jcat.2001.3234.
68. VOC catalyst with Noble metal. https://www.hnxintan.com/product/VOC-catalyst-with-Noble-metal--54.html.
69. Kucharczyk, B., Stasińska, B., and Nawrat, S. (2017). Studies on work of a prototype installation with two types of catalytic bed in the reactor for oxidation of methane from mine ventilation air. FUEL PROCESSING TECHNOLOGY *166*, 8-16. 10.1016/j.fuproc.2017.05.026.
70. Gosiewski, K., Pawlaczyk, A., and Jaschik, M. (2015). Energy recovery from ventilation air methane via reverse-flow reactors. Energy *92*, 13-23. https://doi.org/10.1016/j.energy.2015.06.004.
71. Ravel, B., and Newville, M. (2005). ATHENA, ARTEMIS, HEPHAESTUS: data analysis for X-ray absorption spectroscopy using IFEFFIT. J. Synchrotron Radiat. *12*, 537-541. 10.1107/S0909049505012719.

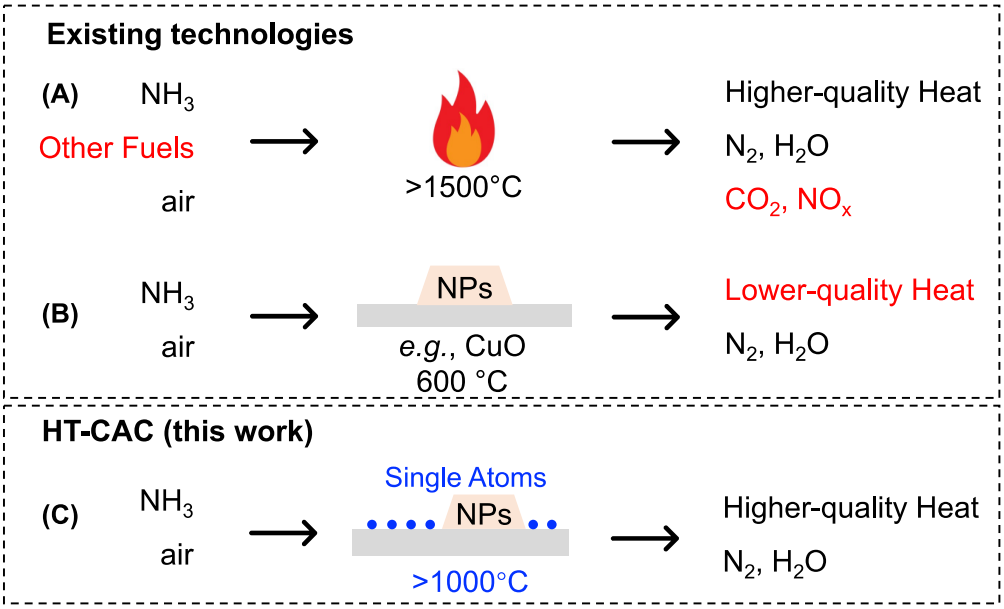

Figure 1. Schematic comparison of the HT-CAC with existing main approaches for NH_3 combustion. Existing technologies include (A) co-firing NH_3 with conventional fossil fuels in high-temperature flame combustion, providing high-quality energy but resulting in CO_2 and NO_x emissions.; (B) NH_3 catalytic combustion that can achieve low NO_x emissions either at relatively low reaction temperatures (e.g., 600°C) or under undesired fuel-rich conditions. (C) This work introduces high-temperature catalytic NH_3 combustion (HT-CAC) enabled by single-atom catalysts (with large particle spectators). HT-CAC can selectively convert NH_3 and air to N_2 and H_2O under fuel-lean conditions and at temperatures above 1000°C, ensuring high-quality heat generation while minimizing NO_x pollution.

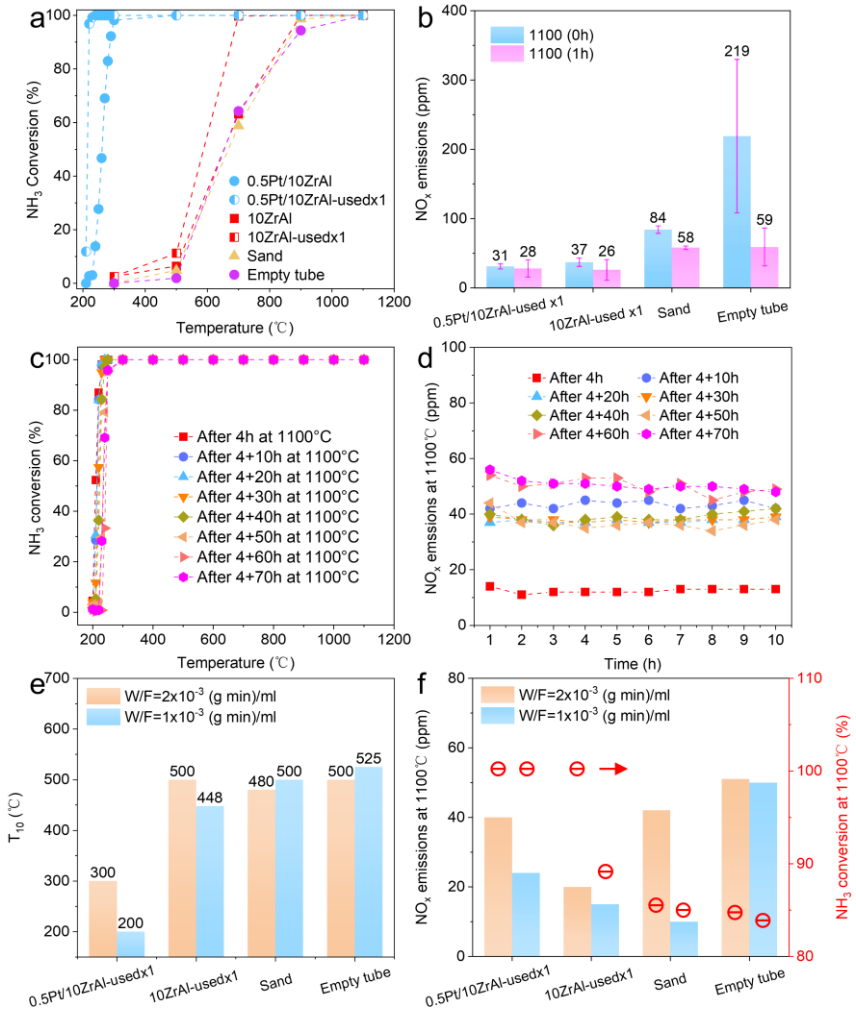

Figure 2. HT-CAC performance of 0.5Pt/10ZrAl. (A) NH_3 combustion light-off curves for various catalysts, including fresh 0.5Pt/10ZrAl, 0.5Pt/10ZrAl-usedx1, bare 10ZrAl, 10ZrAl-usedx1, sand only, and an empty tube. (B) NO_x emissions measured at 1100°C nominal temperature (at the 0-hour mark) and after stabilization (at the 1-hour mark). Error bars indicate standard deviations from three independant tests. A more complete set of data can be found in **Table S1**. (C) Light-off curves of 0.5Pt/10ZrAl-usedx1 during consecutive 10-hour tests; feed gas was switched to Ar between runs. (D) NO_x emissions during each 10-hour test cycle. Reaction conditions for (A–D): 2 vol.% NH_3, 3 vol.% O_2, Ar balance, 100 mL/min flow rate, W/F = 2×10^{-3} g·min/mL, GHSV = 5500 h^{-1}. (E–F) HT-CAC performance with N_2 as the balancing gas. (E) NH_3 conversions at 1100°C for 0.5Pt/10ZrAl-usedx1 under standard (W/F = 2×10^{-3} g·min/mL) and high flow rate (W/F = 1×10^{-3} g·min/mL) conditions, compared to 10ZrAl-usedx1, sand only, and an empty tube. (F) NO_x emissions and NH_3 conversions at 1100°C after 1 hour of reaction (**Table S2**). Reaction conditions for (E–F): 2 vol.% NH_3, 15 vol.% air, N_2 balance; flow rates of 100 mL/min (GHSV = 5500 h^{-1}) and 200 mL/min (GHSV = 11,000 h^{-1}).

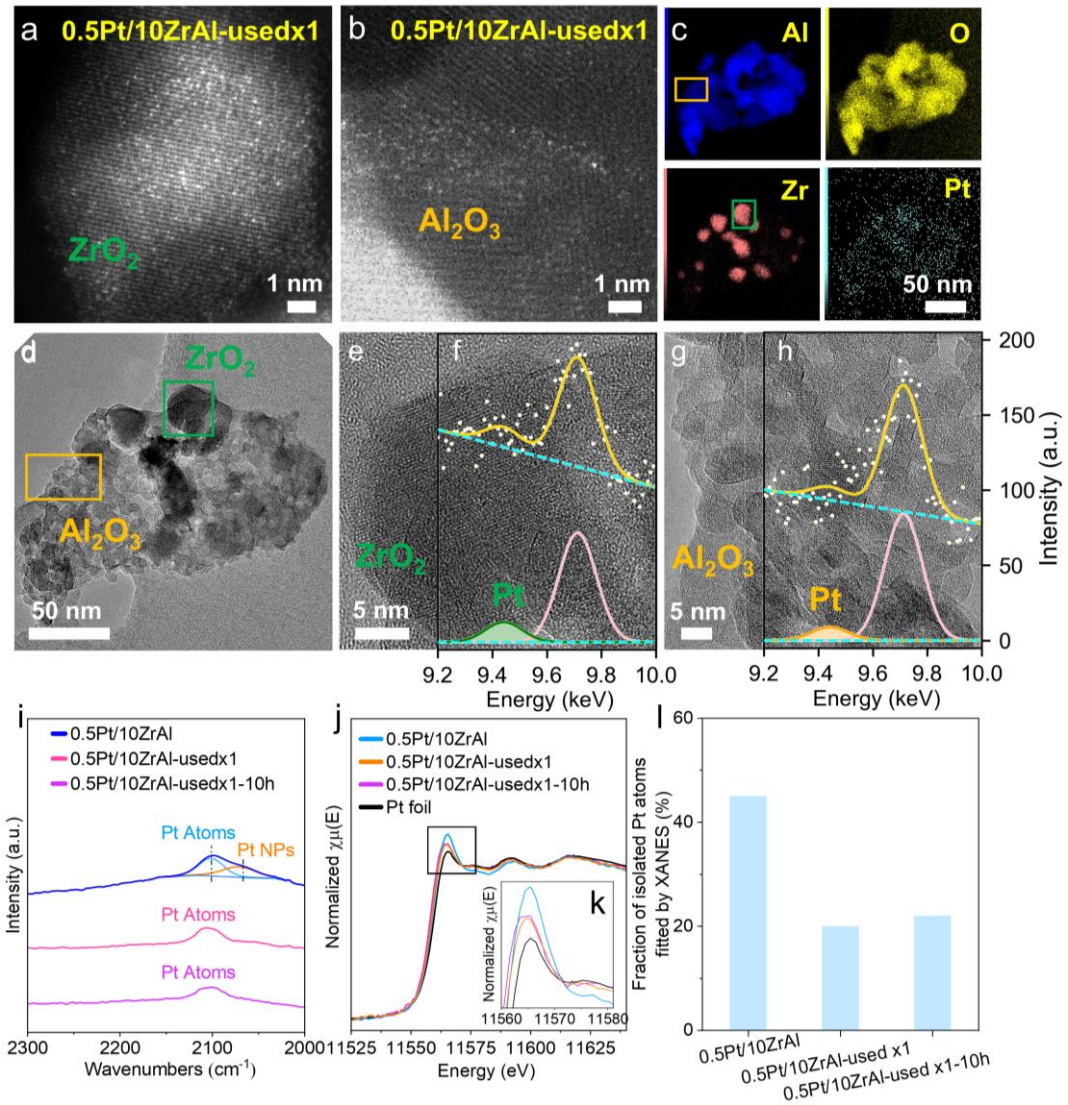

Figure 3. Characterization the 0.5Pt/10ZrAl catalyst before and after HT-CAC. (A, B) STEM-HAADF images of the 0.5Pt/10ZrAl-usedx1 catalyst. (C) STEM-XEDS mapping. (D-H) Representative TEM image and the corresponding STEM-XED spectra. Additional images and X-EDS maps of the fresh 0.5Pt/10ZrAl catalyst can be found in **Figure S12**. Full X-EDS spectra for (E, F) are displayed in **Figure S14**. Additional STEM-HAADF images after 80-hour stability testing are in **Figure S19**. (I) CO-DRIFTS spectra of 0.5Pt/10ZrAl, 0.5Pt/10ZrAl-usedx1 and 0.5Pt/10ZrAl-usedx1-10h after in situ heat treatment in 5 vol.% H_2/N_2 at 300°C for 60 minutes. (J, K) XANES spectra of fresh and used catalysts with reference Pt foil and a magnified region. (L) The fraction of isolated Pt atom estimated from fitting XANES curves (detailed in **Figure S18**), using spectra from reference samples of Pt single atoms (**Figure S17**) and Pt foil.

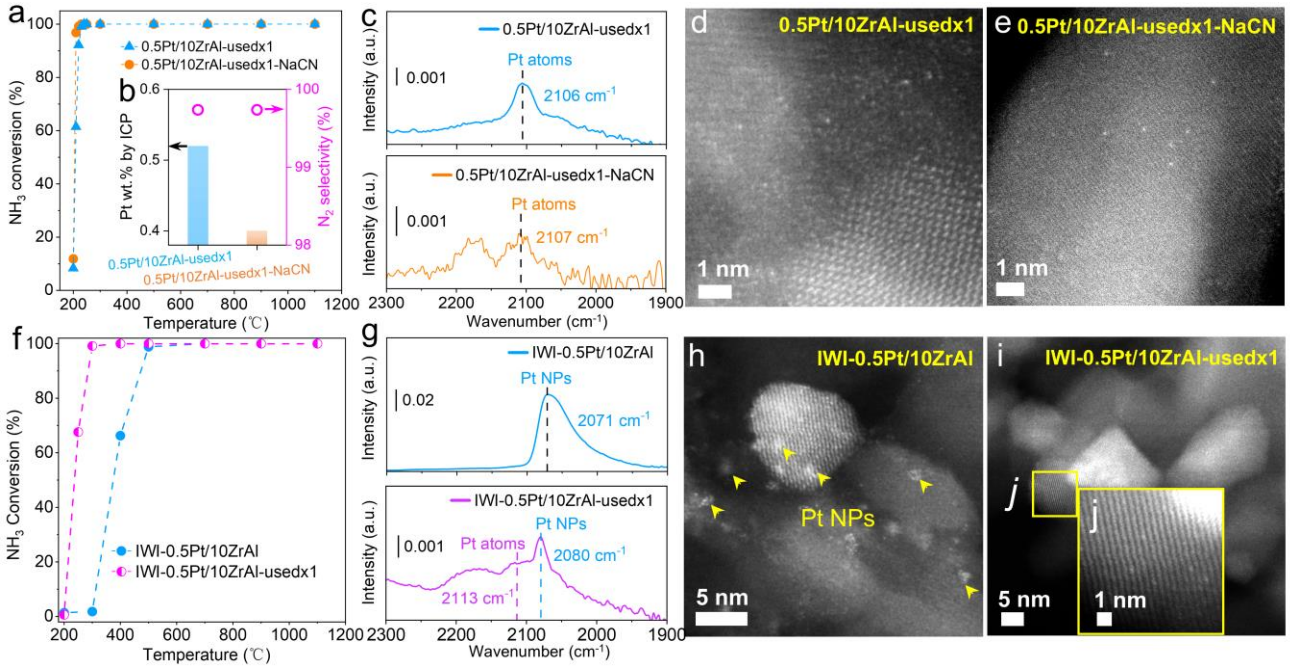

Figure 4. Catalytic performance and structural characterization of model catalysts. (A) Ammonia combustion light-off curves for 0.5Pt/10ZrAl-used x1 before and after 40°C etching in 2 wt.% NaCN solution for 6 hours. (B) Pt weight percent (wt.%) and N_2 selectivity of 0.5Pt/10ZrAl-used x1 before and after etching (1-hour mark at 1100°C). Additional N_2 selectivity data is in **Figure S23**. Reaction conditions: 2 vol.% NH_3, 3 vol.% O_2, Ar balance, 100 mL/min, W/F = 2×10^{-3} g·min/mL, GHSV = 5500 h^{-1}. (C) CO-DRIFTS spectra of 0.5Pt/10ZrAl-usedx1 before and after NaCN etching, recorded after in situ heat treatment in 5 vol.% H_2/N_2 at 300°C. (D, E) STEM-HAADF images of 0.5Pt/10ZrAl-usedx1 before (D) and after (E) etching. Additional images are in **Figure S24**. (F) Ammonia combustion light-off curves for IWI-0.5Pt/10ZrAl and IWI-0.5Pt/10ZrAl-usedx1. Corresponding N_2 selectivity is in **Table S1**. (G) CO-DRIFTS spectra of IWI-0.5Pt/10ZrAl and IWI-0.5Pt/10ZrAl-usedx1 after in situ heat treatment with 5 vol. % H_2/N_2 at 300°C for 60 minutes. (H) STEM-HAADF image of IWI-0.5Pt/10ZrAl with small Pt nanoparticles highlighted (yellow arrows). (I, J) STEM-HAADF image of IWI-0.5Pt/10ZrAl after HT-CAC, with (J) showing a magnified region from (I).

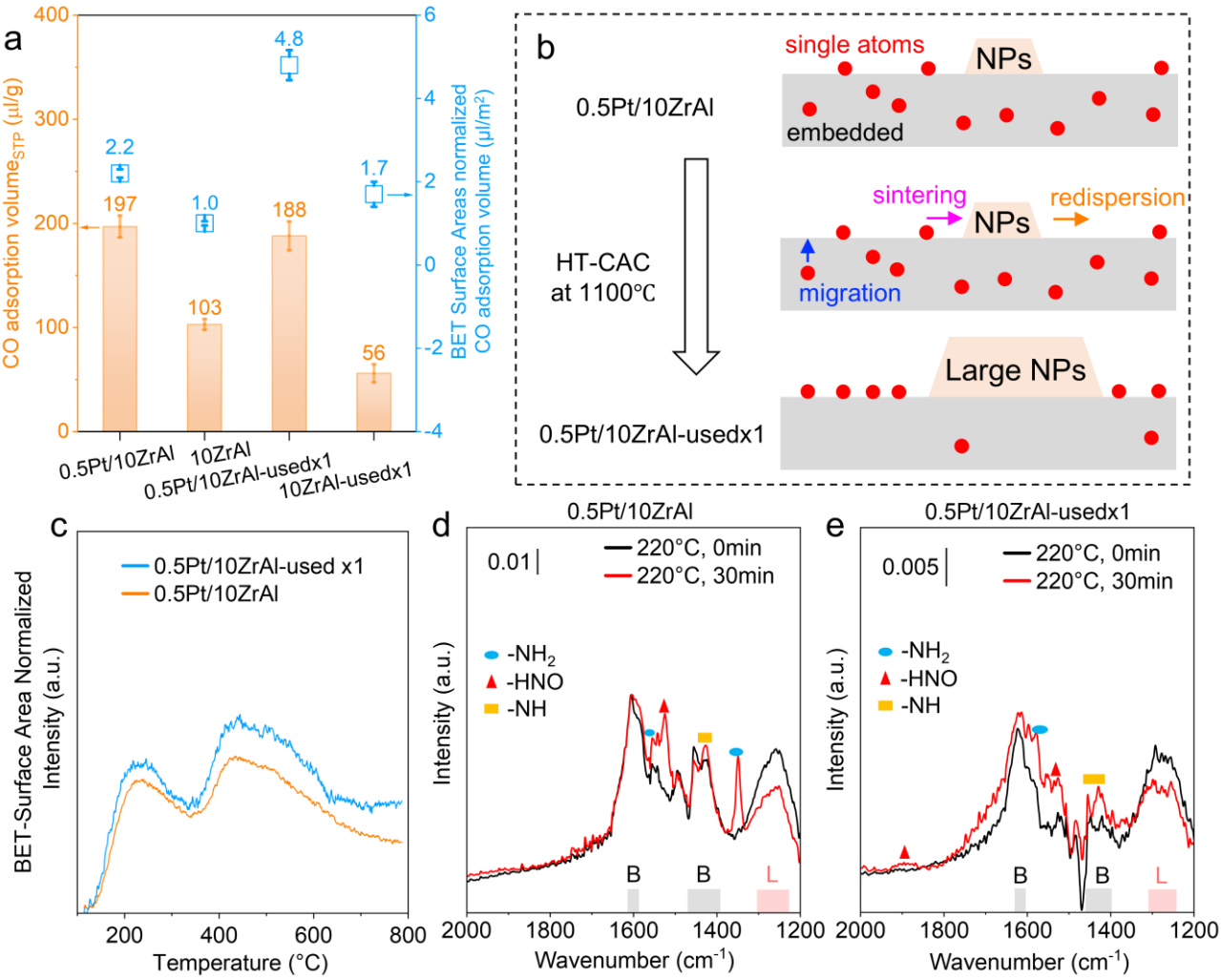

Figure 5. Investigating the in situ activation effect of the 0.5Pt/10ZrAl catalyst for HT-CAC. (A) CO adsorption volume (µL) and CO adsorption normalized by BET surface area (µL/(m²·g)) from CO pulse titration tests of 0.5Pt/10ZrAl materials at 50°C. CO titration was conducted after reduction at 300°C for 60 minutes in 5 vol.% H_2/N_2, followed by cooling to 50°C for titration cycles. (B) Schematic representation of the possible evolution of 0.5Pt/10ZrAl during the 1st run of HT-CAC. (C) O_2-TPD profiles of 0.5Pt/10ZrAl and 0.5Pt/10ZrAl-usedx1 (D, E) In situ NH_3-DRIFTS spectra showing the reactivity of adsorbed NH_3 species with 3 vol.% O_2/Ar at 220°C for (D) fresh 0.5Pt/10ZrAl and (E) 0.5Pt/10ZrAl-usedx1 catalysts. Additional details can be found in **Figures S29** and **S30**. The NH_3-absorption bands on B-acid sites and L-acid sites, as well as IR features for intermediates are highlighted, according to the literature.

Supplementary Information

Single Atom Catalysts-Enabled Catalytic Ammonia Combustion at Above 1000℃

Yankun Du,[1,†] Bingqing Yao,[1,†] Liang Xu,[1] Shangchen Lu,[1] Chaokai Xu,[1] Peijie Han[2], Sheng Dai,[3] Sikai Wang,[2] Shibo Xi,[4] Ning Yan[2,5*] and Qian He[1,5*]

1 Department of Material Science and Engineering, College of Design and Engineering, National University of Singapore, 9 Engineering Drive 1, EA #03-09, Singapore, 117575w

2 Department of Chemical and Biomolecular Engineering, College of Design and Engineering, National University of Singapore, 4 Engineering Drive 4, E5 #02-29, Singapore, 117585

3 Key Laboratory for Advanced Materials and Joint International Research Laboratory of Precision Chemistry and Molecular Engineering, School of Chemistry and Molecular Engineering, East China University of Science & Technology, Shanghai 200237, China

4 Institute of Sustainability for Chemicals, Energy and Environment (ISCE2), Agency for Science, Technology and Research in Singapore (A*STAR), 1 Pesek Road, Jurong Island 627833, Singapore

5 Centre for Hydrogen Innovations, National University of Singapore, E8, 1 Engineering Drive 3, Singapore, 117580

*Corresponding authors: Ning Yan (NY) ning.yan@nus.edu.sg; Qian He (QH): heqian@nus.edu.sg

† These authors contributed equally.

Table of contents

Table S1. HT-CAC performance in Ar balance. Reaction conditions: 2 vol.% NH_3, 3 vol.% O_2, Ar balance, in total 100 mL/min, W/F_{total}= $2x10^{-3}$ (g min)/ml, GHSV= 5500 h^{-1}.

Entry	Samples	Activity (°C)		NH_3 conversion at 1100°C at the 0h mark (%)	Selectivity (%) at 1100°C at the 0h mark			NO_x emissions at 1100°C at the 0h mark (ppm)	NO_x emissions at 1100°C at the 1h mark (ppm)
		T_{10}	T_{90}		N_2	N_2O	NO		
1	Al_2O_3	490	570	100	98.56	0.00	1.44	~138	~14
2	ZrO_2	500	675	100	99.20	0.44	0.36	~82	~75
3	Sand	540	870	100	99.09	0.32	0.59	~80	~58
4	Empty tube	600	880	100	98.89	0.37	0.74	~104	~59
5	10ZrAl (10%ZrO_2-Al_2O_3)	470	600	100	99.64	0.19	0.18	~35	~33
6	10ZrAl-used x1	500	670	100	99.67	0.09	0.24	~30	~26
7	0.5Pt/10ZrAl	236	284	100	79.28	0.00	20.72	~2153	~29
8	0.5Pt/10ZrAl-usedx1	210	215	100	99.66	0.17	0.17	~34	~28
9	0.5Pt/10ZrAl-usedx2	212	216	100	-	-	-	-	-
10	0.5Pt/Al_2O_3	246	296	100	56.22	0.30	43.49	~5141	~47
11	0.5Pt/Al_2O_3-usedx1	234	240	100	90.42	0.24	9.34	~93	~43
12	0.5Pt/10ZrAl-usedx1-NaCN	200	219	100	96.98	0.14	2.89	~335	~31
13	IWI-0.5Pt/10ZrAl	310	435	100	77.26	0.00	22.74	~2402	~2844
14	IWI-0.5Pt/10ZrAl-usedx1	230	270	100	84.57	0.10	15.33	~1582	~455

Note: NH_3 conversion, selectivity, and NO_x emissions at 1100°C represent average values derived from data collected at two specific time intervals: the 0-hour mark (minutes 0-10) and the 1-hour mark (minutes 55-65). The 0-hour mark indicates the furnace has just reached the nominal temperature of 1100°C, while the 1-hour mark reflects conditions after maintaining 1100°C for approximately one hour.

Table S2. HT-CAC performance in N_2 balance, and different flow rates

Entry	Samples	Activity (℃)		NH_3 conversion at 1100℃ at the 0-hour mark (%)	NO_x emissions at 1100℃ at the 0-hour mark (ppm)	NH_3 conversion at 1100℃ at the 1-hour mark (%)	NO_x emissions at 1100℃ at the 1-hour mark (ppm)	Reaction conditions
		T_{10}	T_{90}					
1	0.5Pt/10ZrAl	300	500	100	~33	100	~25	
2	0.5Pt/10ZrAl-usedx1	300	830	100	~40	100	~34	2 vol. % NH_3 15 vol. % Air N_2 balance **100ml/min in total** **W/F_{total}= 2x10^{-3} (g min)/ml)** **GHSV= 5500 h^{-1}**
3	10ZrAl (10%ZrO_2-Al_2O_3)	500	1050	100	~31	100	~12	
4	10ZrAl-usedx1	500	1070	100	~20	100	~12	
5	Sand	480	-	86.4	~42	86.0	~38	
6	Empty tube	600	1060	85.2	~52	83.4	~50	
7	0.5Pt/10ZrAl	300	980	99.6	~26	100	~13	
8	0.5Pt/10ZrAl-usedx1	200	840	100	~24	100	~19	2 vol. % NH_3 15 vol. % Air N_2 balance **200ml/min in total** **W/F_{total}= 1x10^{-3} (g min)/ml)** **GHSV= 11000 h^{-1}**
9	10ZrAl (10%ZrO_2-Al_2O_3)	495	995	97.0	~13	100	<10	
10	10ZrAl-usedx1	448	-	87.9	~15	90.7	<10	
11	Sand	500	-	85.6	<10	82.8	<10	
12	Empty tube	525	-	84.1	~51	82.5	~50	

Note: NH_3 conversion, selectivity, and NO_x emissions at 1100℃ represent average values derived from data collected at two specific time intervals: the 0-hour mark (minutes 0-10) and the 1-hour mark (minutes 55-65). The 0-hour mark indicates the furnace has just reached the nominal temperature of 1100℃, while the 1-hour mark reflects conditions after maintaining 1100℃ for approximately one hour.

Table S3. ICP-OES results of Hf content in $ZrO(NO_3)_2 \cdot xH_2O$ and 0.5Pt/10ZrAl materials.

Sample	Zr precursor	Hf content
$ZrO(NO_3)_2 \cdot xH_2O$-S	Sigma, 99%	0.51%
0.5Pt/10ZrAl-S	Sigma, 99%	0.14%
$ZrO(NO_3)_2 \cdot xH_2O$-A	Aladdin, 99.5%	0.49%
0.5Pt/10ZrAl-A	Aladdin, 99.5%	0.11%

Note: The Zr precursor in 0.5Pt/10ZrAl-S was denoted as $ZrO(NO_3)_2 \cdot xH_2O$-S (Sigma, 99%), while the ZrO_2 precursor in 0.5Pt/10ZrAl-A was denoted as $ZrO(NO_3)_2 \cdot xH_2O$-A (Aladdin, 99.5%).

Table S4. Summary of the EXAFS fitting of Pt L_3-edge of 0.5Pt/10ZrAl related materials.

Sample	N_{Pt-Pt}	R_{Pt-Pt}	σ^2_{Pt-Pt}	N_{Pt-O}	R_{Pt-O}	σ^2_{Pt-O}	R factor
0.5Pt/10ZrAl	12.3±1.3	2.752±0.005	0.0043	1.6±0.6	1.86±0.04	0.0043	0.0074
0.5Pt/10ZrAl-usedx1	11.1±1.6	2.756±0.007	0.0037	1.0±0.7	1.95±0.07	0.0037	0.0139
0.5Pt/10ZrAl-usedx1-10h	11.5±1.6	2.767±0.006	0.0036	0.9±0.6	1.94±0.08	0.0036	0.0126

Table S5. Pt contents in different catalysts and their corresponding T_{90} in HT-CAC.

Sample	Loss of Pt (%) determined from ICP-OES	Atomically dispersed Pt (%) determined from XANES	T_{90}
0.5Pt/10ZrAl	-	45	284°C
0.5Pt/10ZrAl-usedx1	-	20	215°C
0.5Pt/10ZrAl-usedx1-NaCN	23.1	-	219°C
0.5Pt/10ZrAl-usedx1-10h	-	22	225°C

Table S6. The Pt dispersion estimated from CO Chemisorption.

Materials	Amount of catalysts used for CO chemisorption (g)	Volume of the adsorbed CO (µl)	Volume of the adsorbed CO (µl) on Pt	Adsorption stoichiometry for Pt:CO	M_{Pt} (g/mol)	Pt wt.%	Calculated Pt Dispersion (%)
10ZrAl	0.11	11.33	-				
0.5Pt/10ZrAl	0.11	21.67	10.33	1:1	195.08	0.5	16%
10ZrAl-usedx1	0.11	6.17	-				
0.5Pt/10ZrAl-usedx1	0.11	20.67	14.50	1:1	195.08	0.5	23%

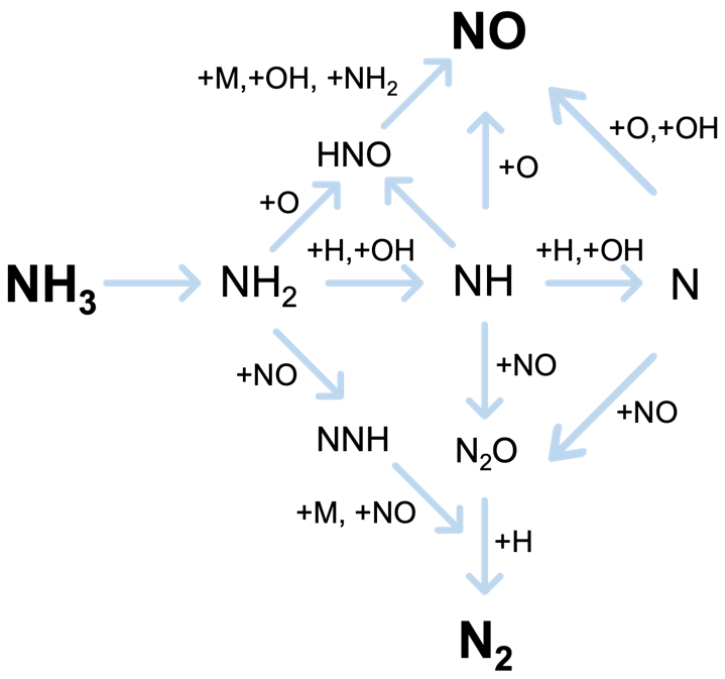

Figure S1. Possible reaction network of NH_3 combustion. Adopted from the J. A. Miller, M. D. Smooke, R. M. Green, R. J. Kee, Kinetic Modeling of the Oxidation of Ammonia in Flames. Combust. Sci. Technol. 34, 149-176 (1983).

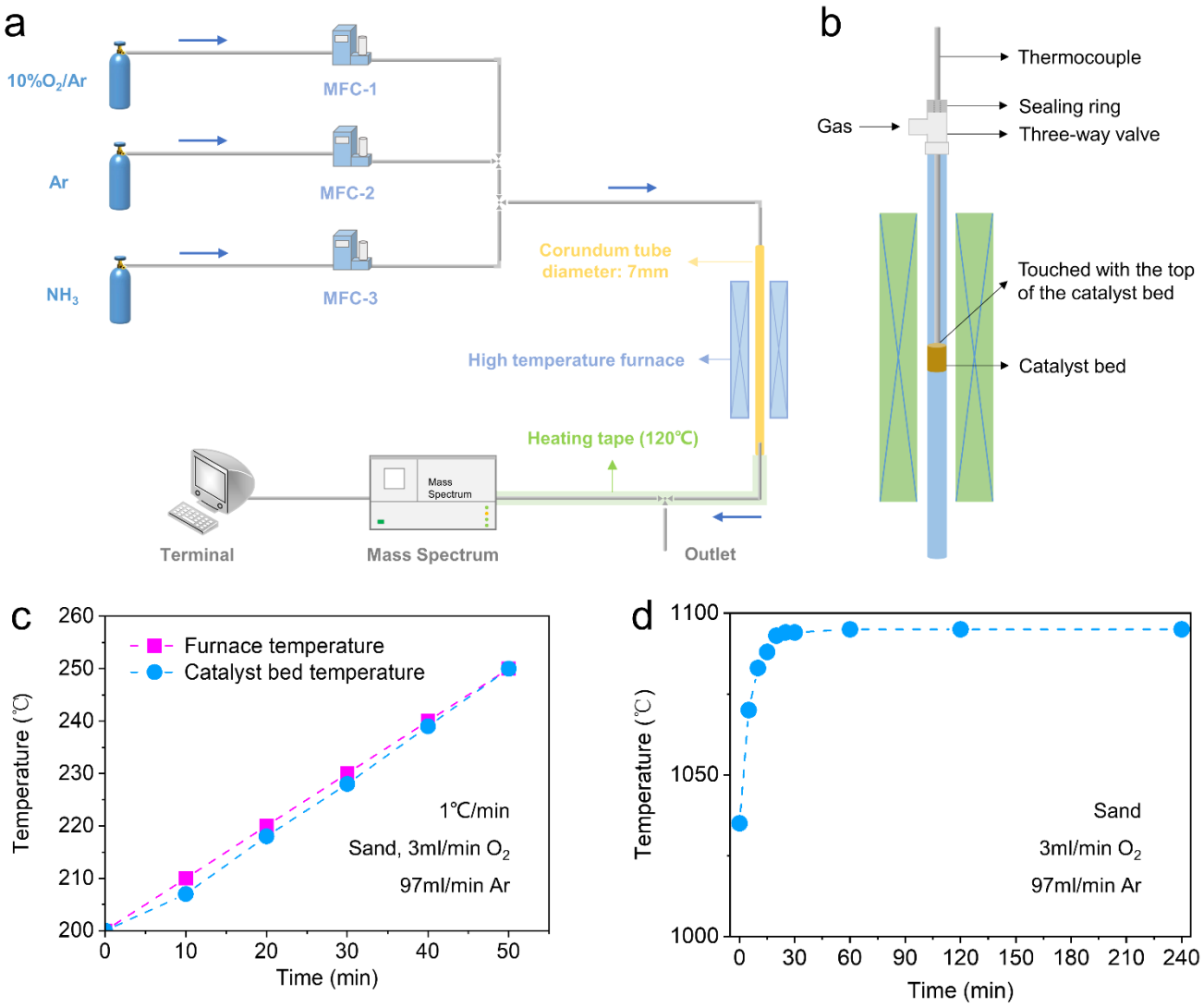

Figure S2. (A) Schematic experimental setup of the reaction system. (B) Schematic of the temperature measurement setup in the laboratory. (C) Comparison of temperatures between the furnace and the catalyst bed under test conditions: sand, 3 mL/min O_2, 97 mL/min Ar, and a heating rate of 1°C/min. (D) Temperature measured at the top surface of the catalyst bed as a function of time after the furnace reaches its nominal temperature of 1100°C. The top surface of the catalyst bed stabilizes at approximately 1095°C after about 30 minutes. Test conditions: sand, O_2 3 ml/min, Ar 97 ml/min.

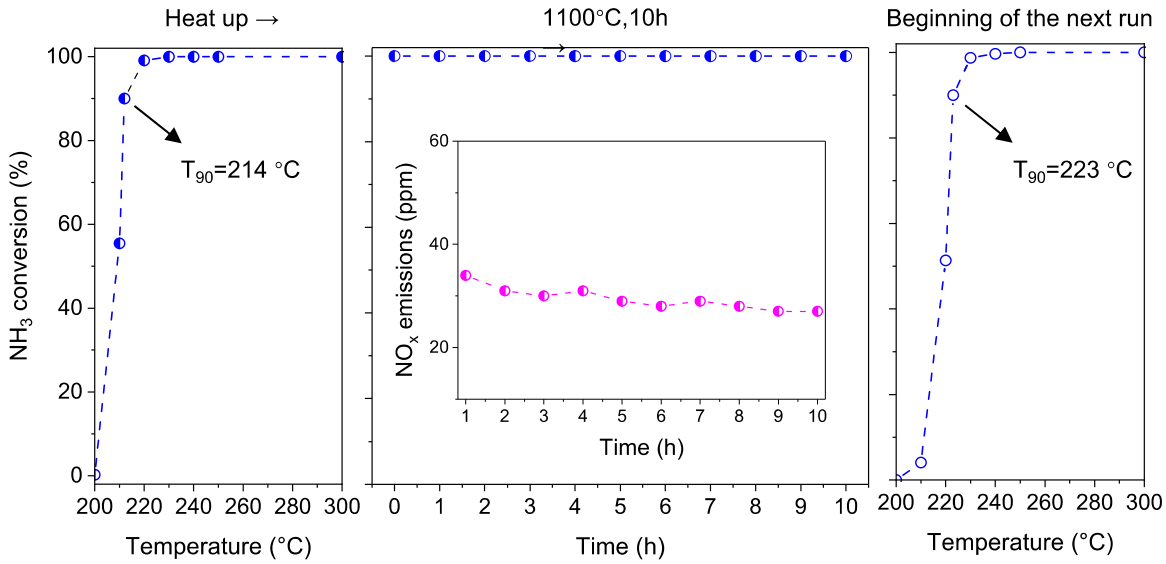

Figure S3. Results of the initial 10-hour stability test for the 0.5Pt/10ZrAl-used x1 material. The left panel presents the light-off curve for its 2nd HT-CAC run, following a prior single use. The reaction was maintained at the target temperature of 1100°C for 10 hours, achieving 100% NH_3 conversion and low NO_x emissions (inlet in the mid-panel) during the extended HT-CAC test. Afterwards, the catalyst was cooled to room temperature before initiating a 3rd HT-CAC run, with its light-off curve shown in the right panel. Typical reaction conditions: 2 vol.% NH_3, 3 vol.% O_2, Ar balance, total flow rate of 100 mL/min, $W/F_{total} = 2 \times 10^{-3}$ (g·min)/mL, GHSV = 15,000 h^{-1}. The reaction temperature was ramped from room temperature to 1100°C and held for 4 hours (unless otherwise specified) at 1100°C under reaction conditions. Detailed information on the HT-CAC test and reaction data is provided in Supplementary Information Table S1.

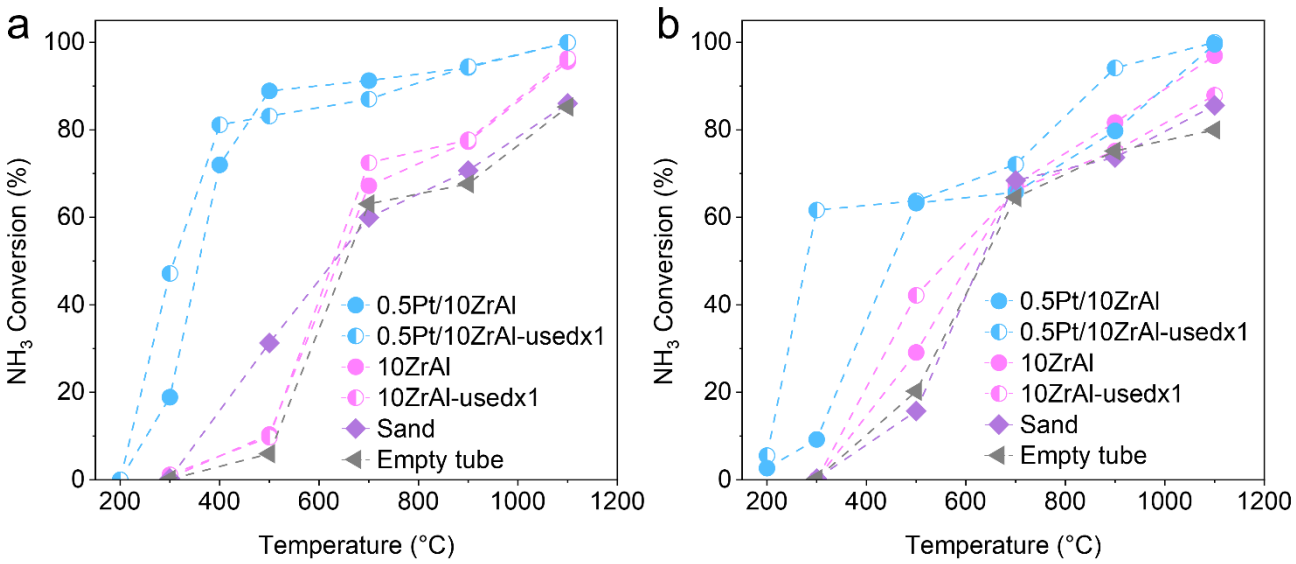

Figure S4. Light-off curves of 0.5Pt/10ZrAl, 0.5Pt/10ZrAl-usedx1, 10ZrAl, 10ZrAl-usedx1, sand, and empty tube in different conditions. (A) 2 vol.% NH_3, 15 vol.% air, N_2 balance, in total 100 mL/min, W/F_{total}= $2x10^{-3}$ (g min)/ml, GHSV= 5500 h^{-1}. (B) 2 vol.% NH_3, 15 vol.% air, N_2 balance, in total 200 mL/min, W/F_{total}= $1x10^{-3}$ (g min)/ml, GHSV= 11000 h^{-1}.

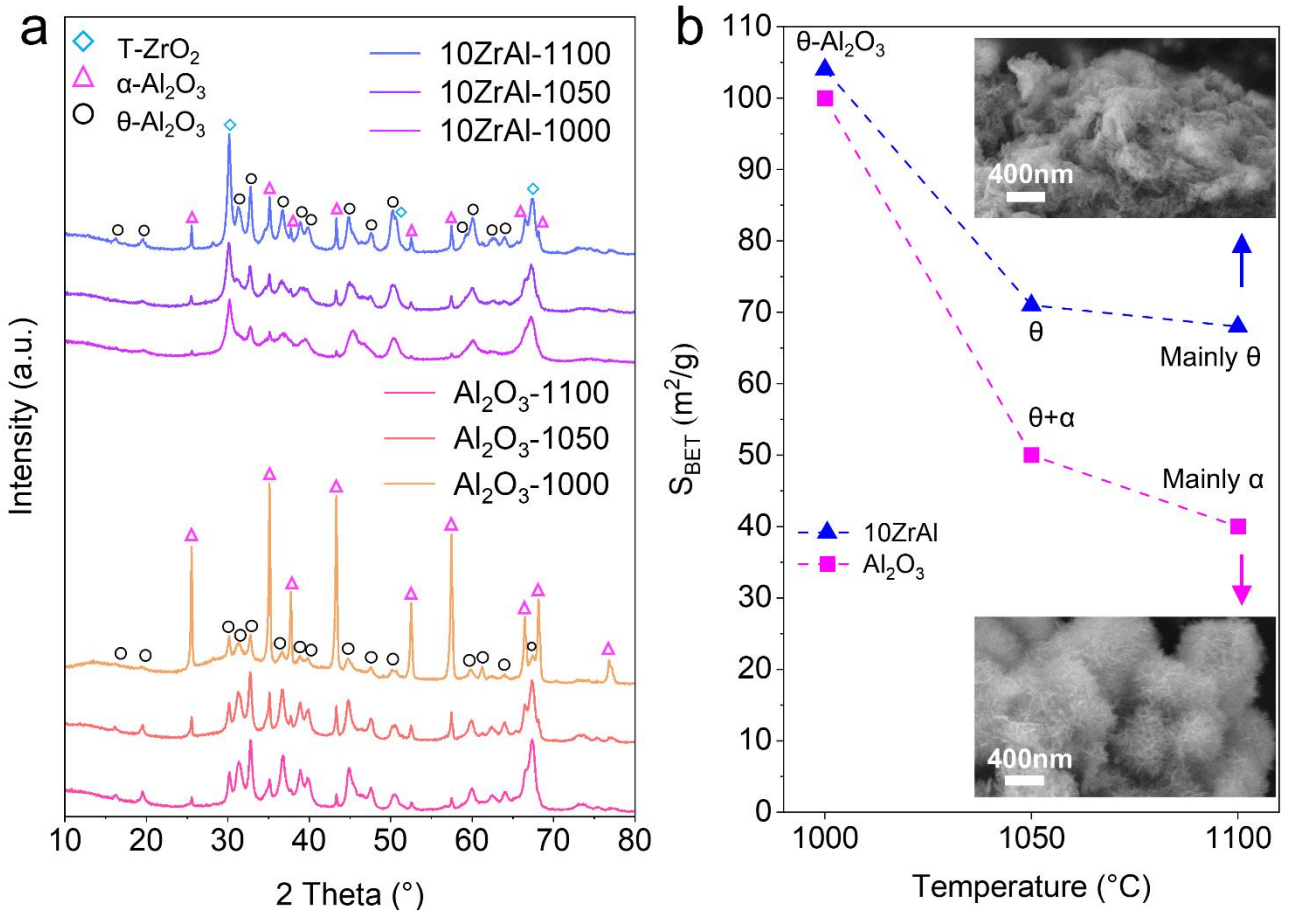

Figure S5. (A) XRD patterns of 10ZrAl and Al_2O_3 (10ZrAl-1000 & Al_2O_3-1000), after calcined at 1050℃ (10ZrAl-1050 & Al_2O_3-1050), and 1100℃ (10ZrAl-1100 & Al_2O_3-1100) in air for 4h, respectively. T-ZrO_2 means the mixed phase of tazheranite and tetragonal ZrO_2, which are difficult to distinguish (b) BET specific surface areas changes and related Al_2O_3 XRD phases of 10ZrAl and Al_2O_3 after calcined at 1000, 1050, and 1100℃ in air for 4h, respectively. The SEM images show the morphology of 10ZrAl and Al_2O_3 after calcined at 1100℃ in air for 4h, respectively.

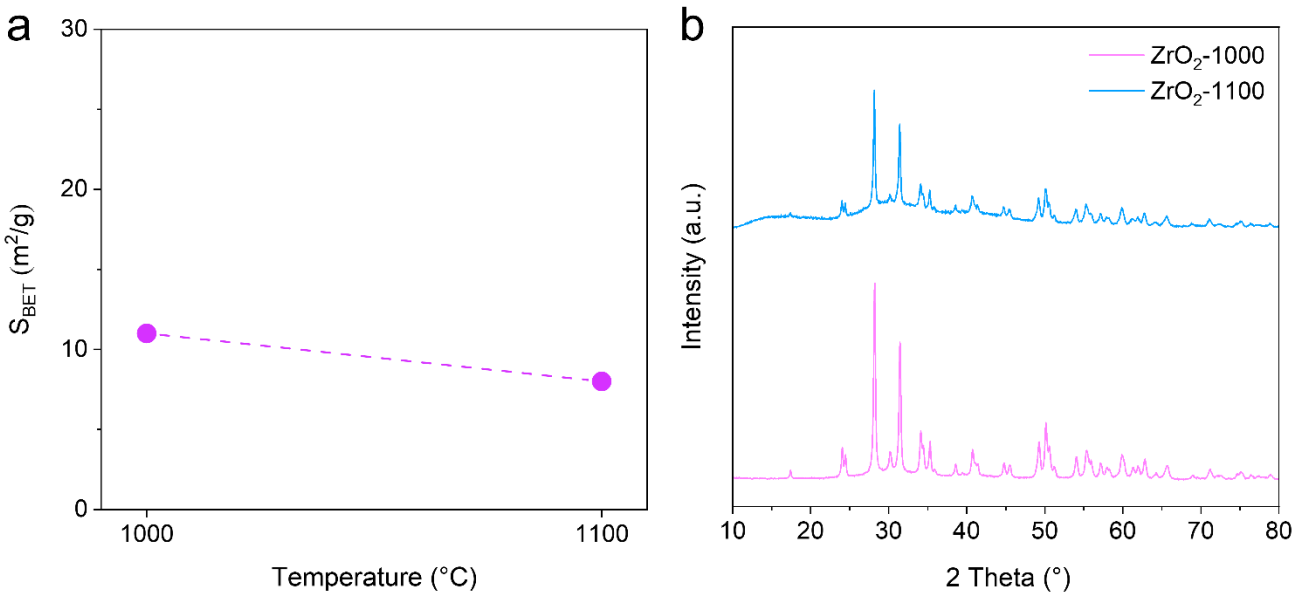

Figure S6. (A) BET specific surface areas and (B) XRD patterns of fresh ZrO_2 (ZrO_2-1000) and after calcined at 1100℃ in air for 4h (ZrO_2-1100), respectively.

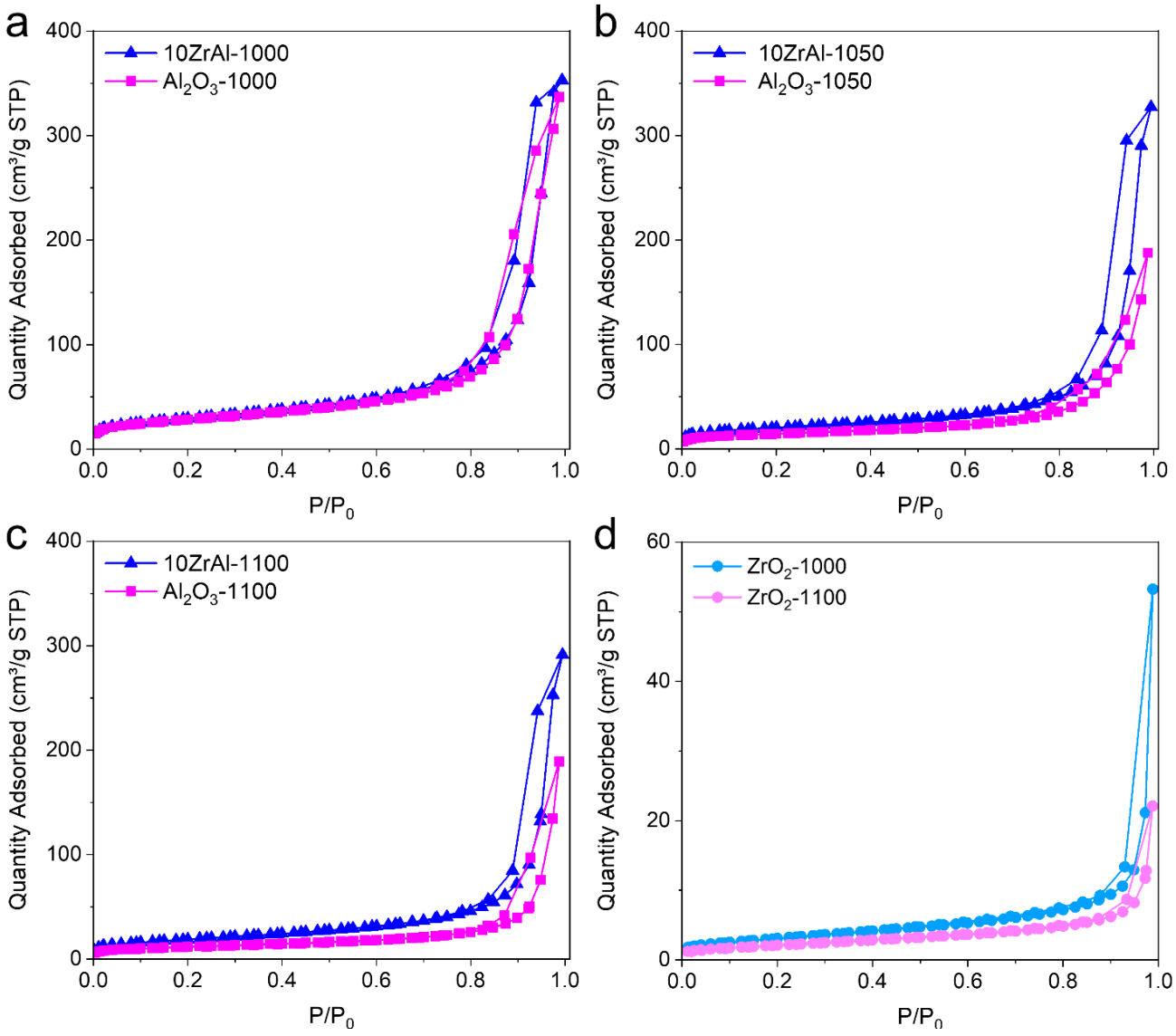

Figure S7. (A-C) N_2 adsorption isotherm analysis of 10ZrAl and Al_2O_3: (A) fresh sample, (B) after calcined at 1050℃ in air for 4h, (C) after calcined at 1100℃ in air for 4h. (D) N_2 adsorption isothermals of fresh ZrO_2 and after calcined at 1100℃ in air for 4h.

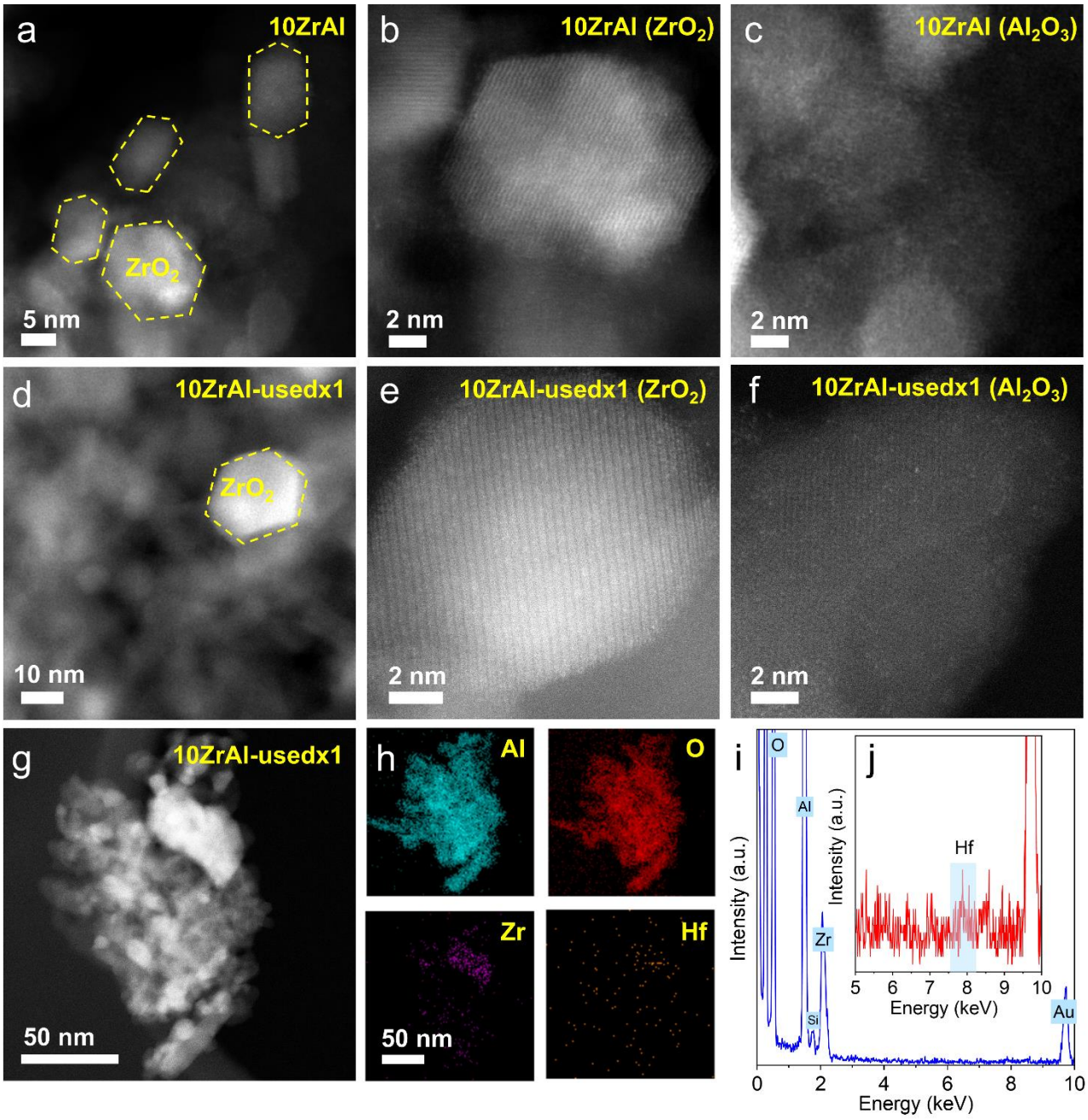

Figure S8. Representative STEM-HAADF images of (A) fresh 10ZrAl, (B) magnified ZrO_2 region in 10ZrAl, and (C) magnified Al_2O_3 region in 10ZrAl. Representative STEM-HAADF images of (D) 10ZrAl-usedx1, (E) magnified ZrO_2 region in 10ZrAl-usedx1, and (F) magnified Al_2O_3 region in 10ZrAl-usedx1. (G, H) The STEM-HADDF image and EDS mappings of 10ZrAl-usedx1 sample. (I) The sum X-ED spectrum from (G) at 0-10.0 keV, and (J) the sum X-ED spectrum at 5-10.0 keV. Detailed Hf weight ratio data can be seen in **Table S3**.

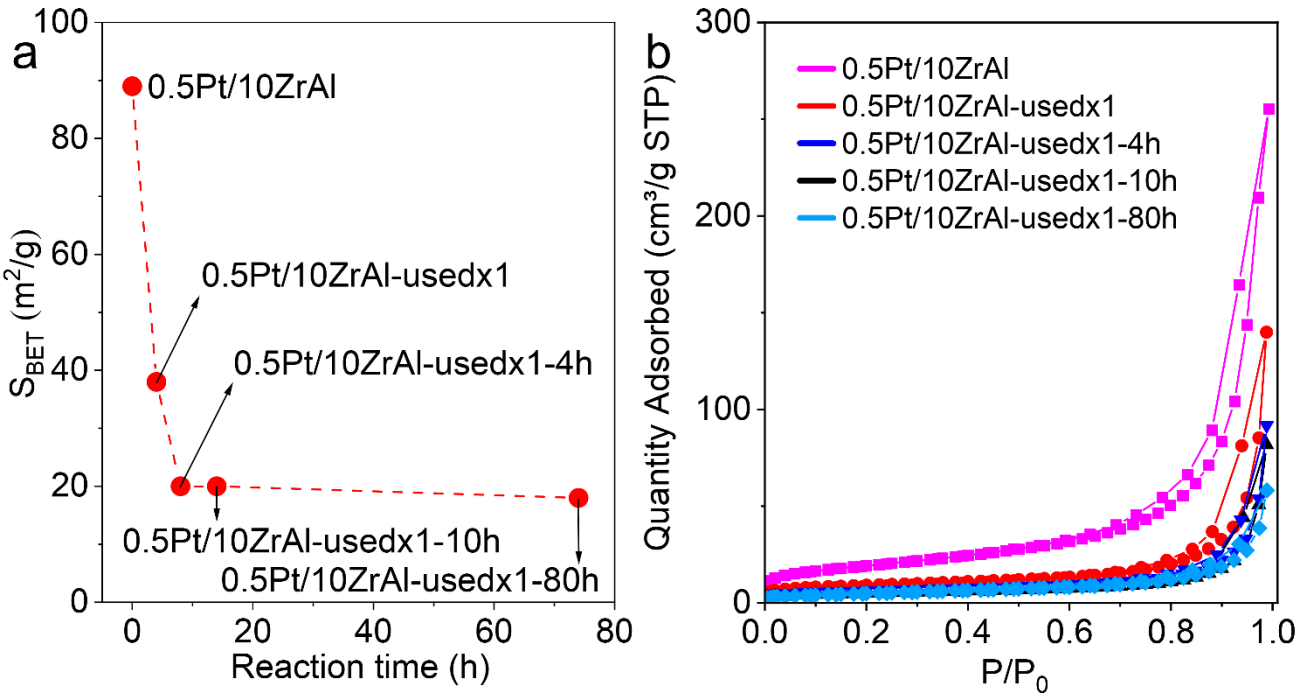

Figure S9. (A) BET specific surface areas and (B) N_2 adsorption isotherm analysis results for the 0.5Pt/10ZrAl, 0.5Pt/10ZrAl-usedx1, 0.5Pt/10ZrAl-usedx1-4h, 0.5Pt/10ZrAl-usedx1-10h and 0.5Pt/10ZrAl-usedx1-80h, respectively.

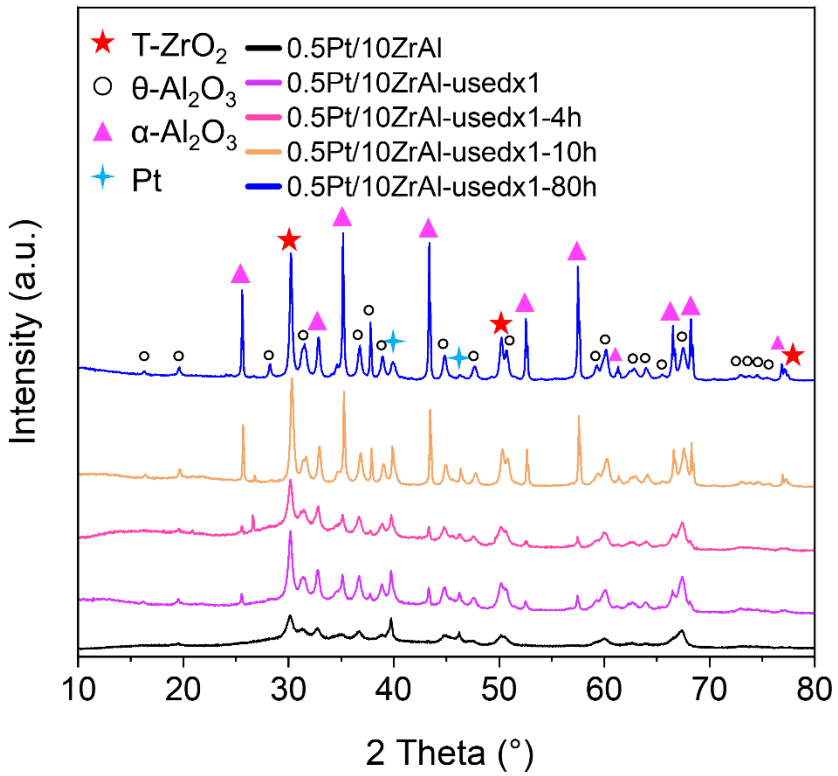

Figure S10. XRD patterns of 0.5Pt/10ZrAl, 0.5Pt/10ZrAl-usedx1, 0.5Pt/10ZrAl-usedx1-4h, 0.5Pt/10ZrAl-usedx1-10h, and 0.5Pt/10ZrAl-usedx1-80h, respectively.

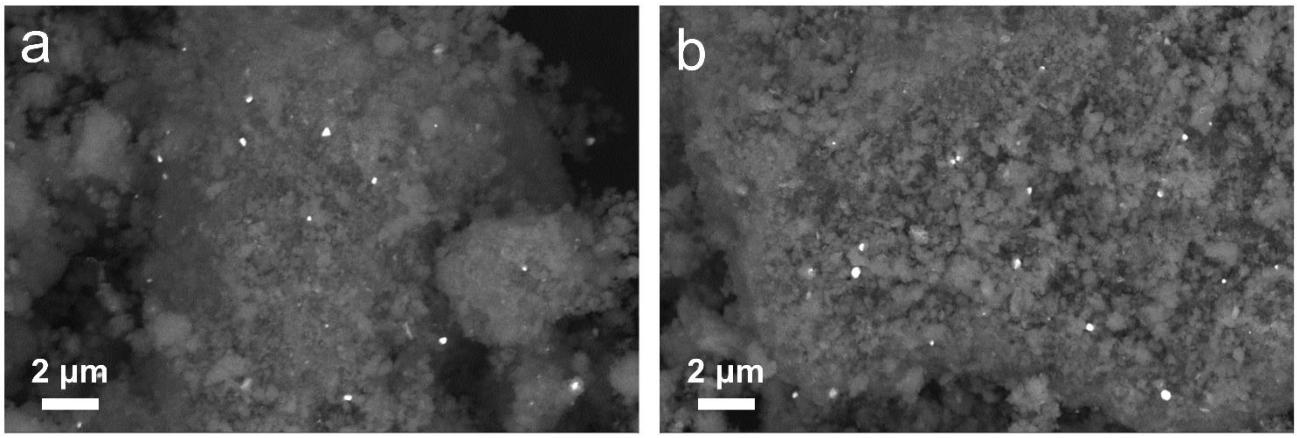

Figure S11. SEM-BSE images of (A) 0.5Pt/10ZrAl and (B) 0.5Pt/10ZrAl-usedx1.

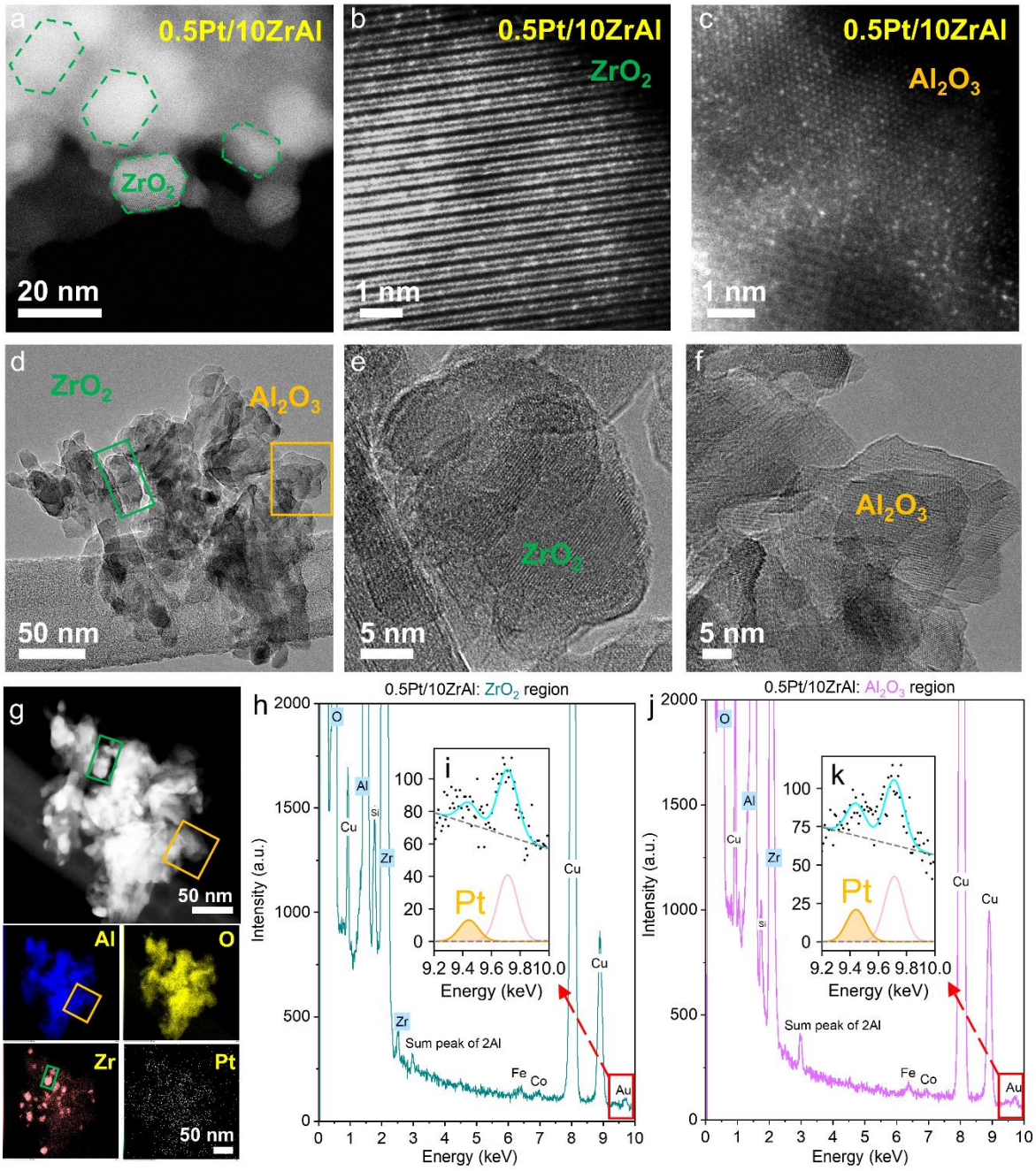

Figure S12. Representative STEM-HAADF images of the fresh 0.5Pt/10ZrAl catalyst (A-C), with ZrO_2 particles highlighted by green dashed lines. TEM-BF images of 0.5Pt/10ZrAl are shown in (D), along with magnified views of the ZrO_2-rich region (E) and the Al_2O_3-rich region (F). The corresponding STEM-XEDS mappings (G) are obtained from the region shown in (D). The summed X-ED spectrum of the ZrO_2 region in (E) is displayed in (H), with a magnified view of the 9.2-10.0 keV range shown in (I). Similarly, the summed X-ED spectrum of the Al_2O_3 region in (F) is presented in (J), with a magnified view in (K). The Au, Fe, and Co signals are likely systematic X-ray artefacts from the instruments, as confirmed by control experiments on carbon support (see **Figure S13**).

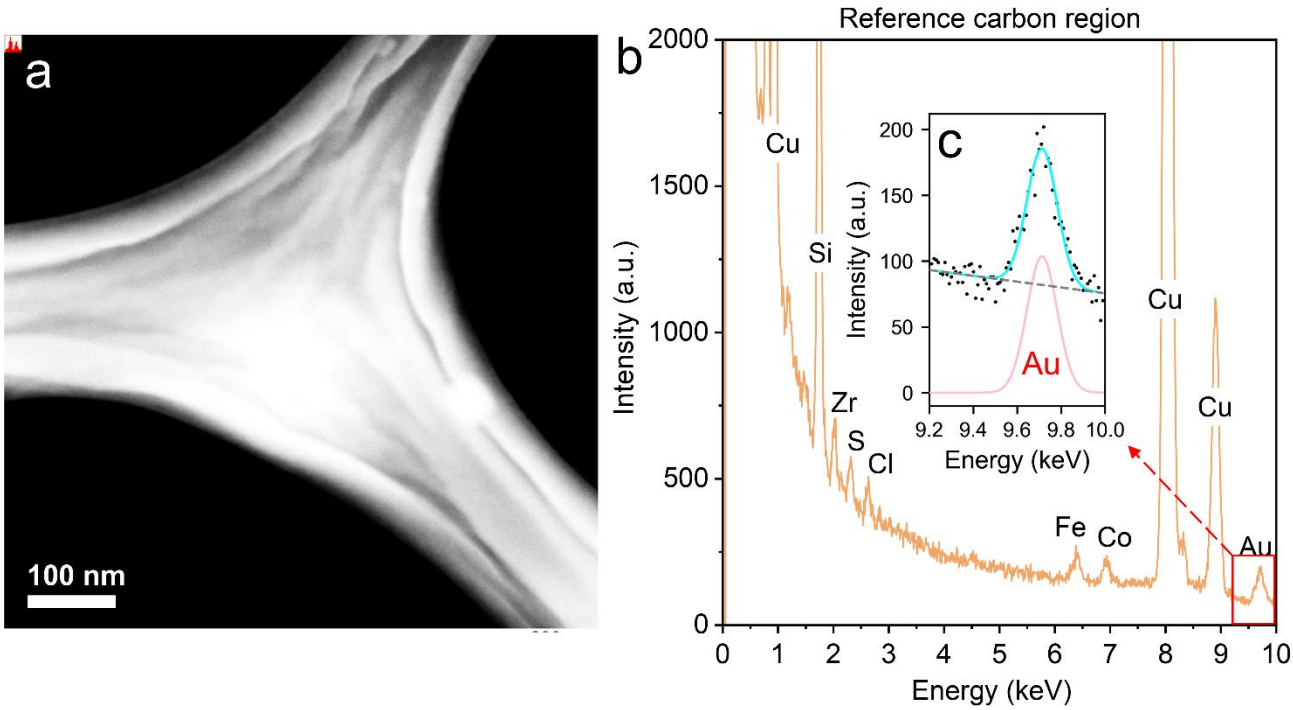

Figure S13. (A) STEM-HAADF image of the reference carbon region. (B) Summed X-ED spectrum from the region shown in (A), with a magnified view of the 9.2-10.0 keV range in (C). No Pt signal was detected in the reference carbon region, and the observed Au signal comes from the microscope.

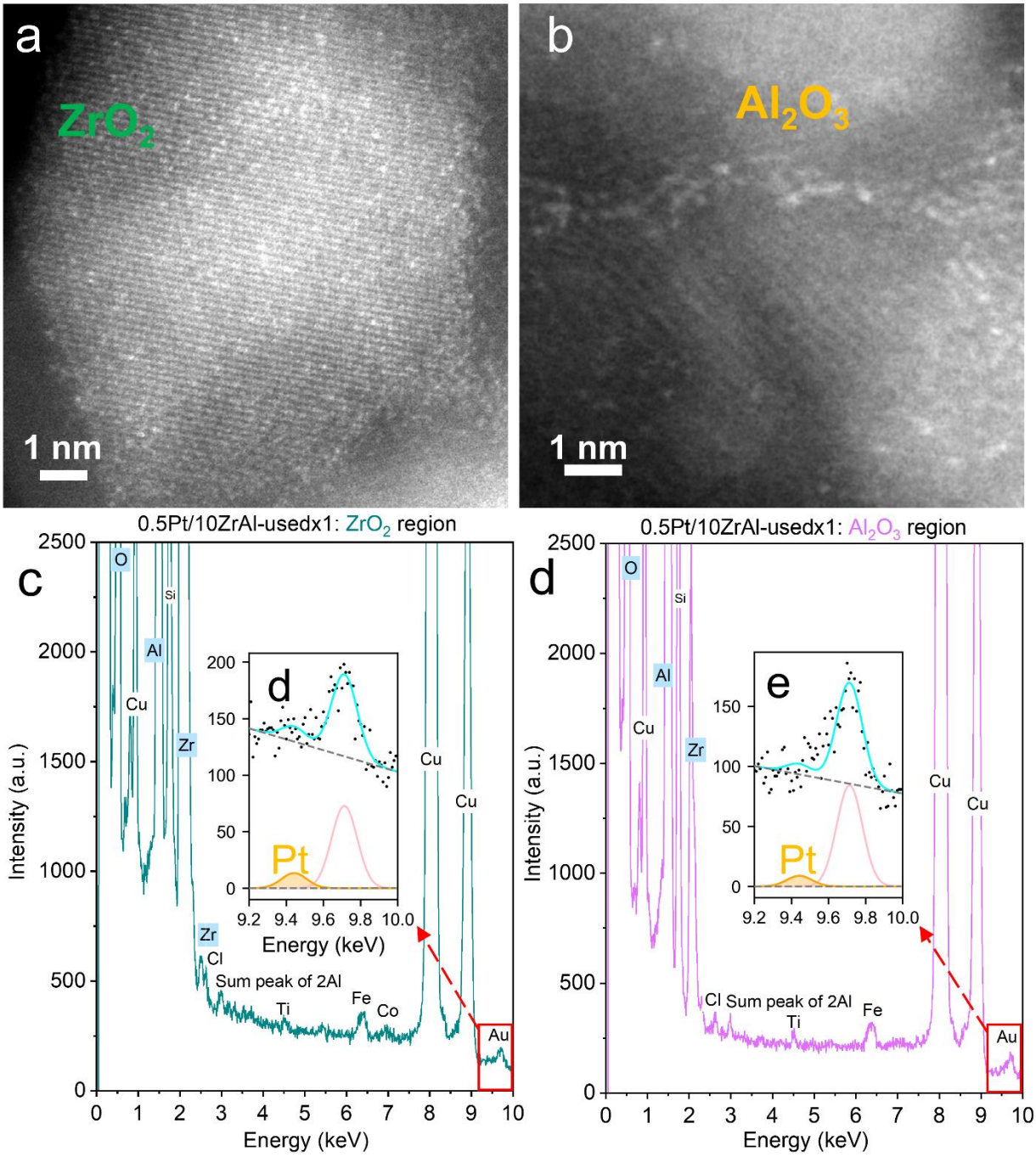

Figure S14. (A, B) STEM-HAADF images of 0.5Pt/10ZrAl-usedx1, showing ZrO_2-rich and Al_2O_3-rich regions, respectively. (C) Summed X-ED spectrum of the ZrO_2 region from **Figure 3E**, with a magnified view of the 9.2-10.0 keV range shown in (D). (E) Summed X-ED spectrum of the Al_2O_3 region from **Figure 3G**, with a magnified view of the 9.2-10.0 keV range shown in (F).

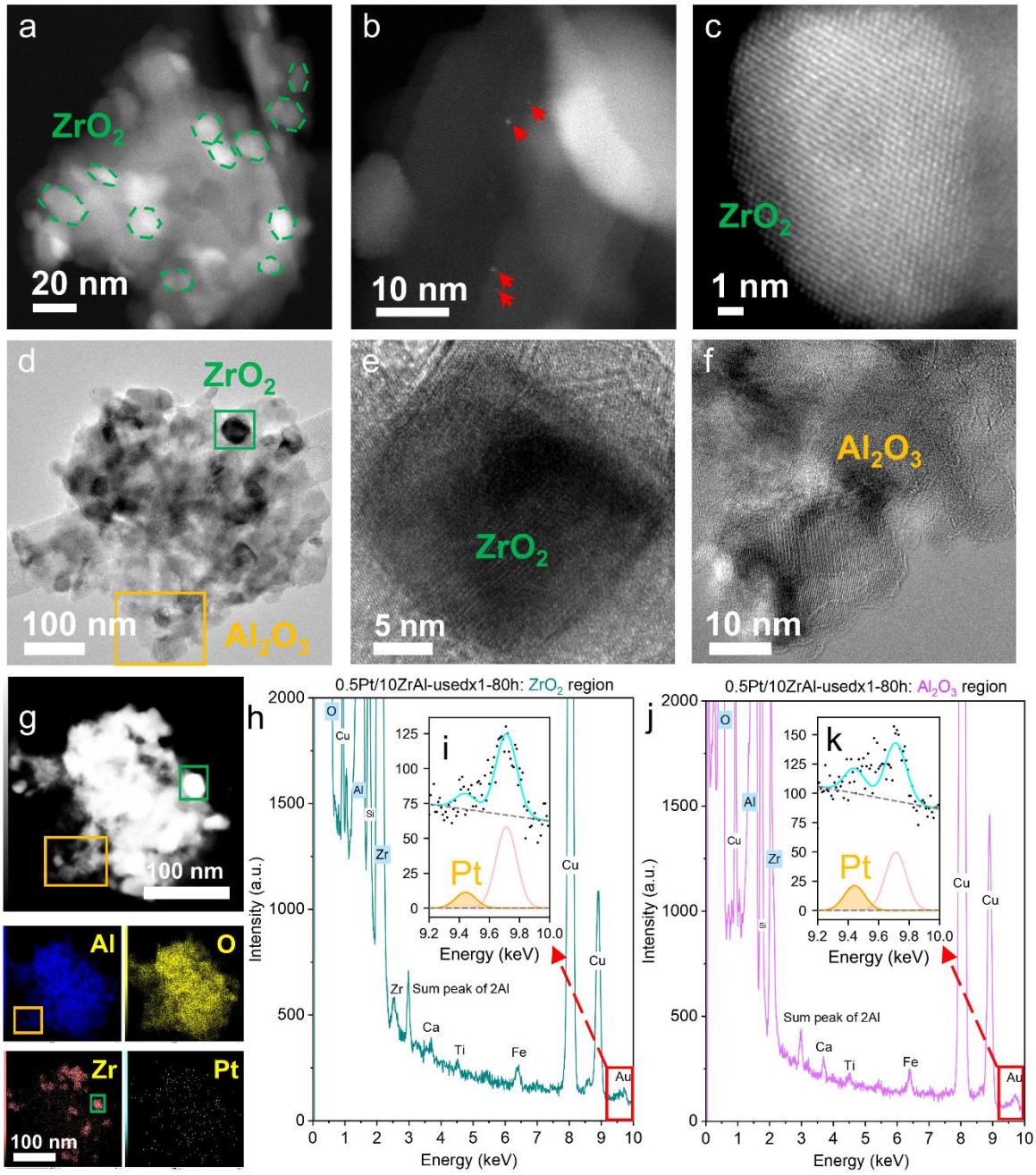

Figure S15. Characterization for the 0.5Pt/10ZrAl-usedx1-80h catalyst. (A-C) Representative STEM-HAADF images, with ZrO_2 particles highlighted by green dashed lines. Small Pt nanoparticles are indicated with red arrows in (B). (D) TEM image of 0.5Pt/10ZrAl-usedx1-80h, with magnified views of the ZrO_2-rich region (E) and the Al_2O_3-rich region (F). (G) EDS mappings corresponding to the TEM region shown in (D). (H) Summed X-ED spectrum of the ZrO_2-rich region from (E), with a magnified view of the 9.2-10.0 keV range in (I). (J) Summed X-ED spectrum of the Al_2O_3-rich region from (F), with a magnified view in (K).

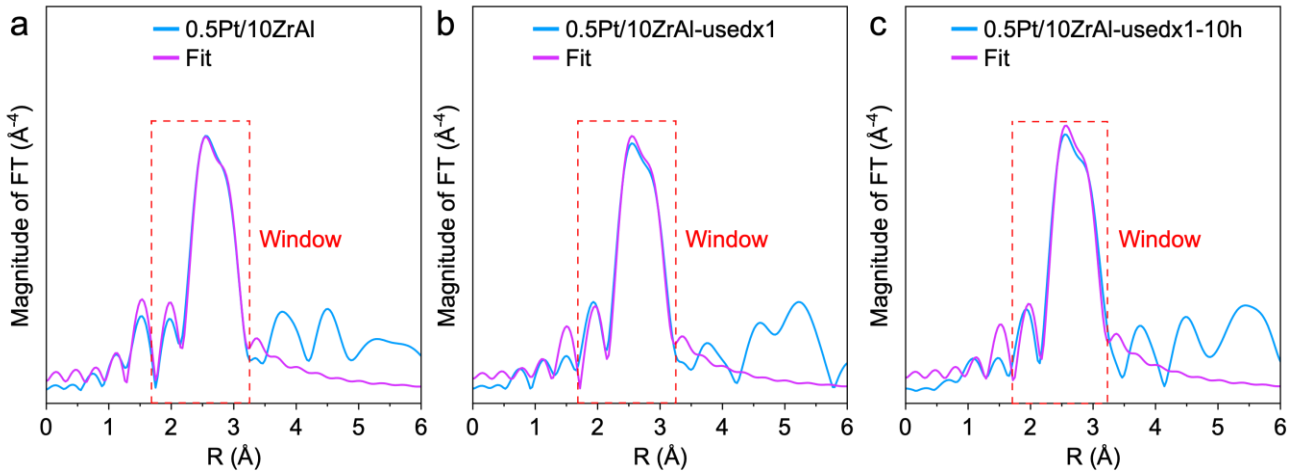

Figure S16. k^3-weighted Fourier transformed Pt L_3-edge EXAFS spectra of (A) 0.5Pt/10ZrAl, (B) 0.5Pt/10ZrAl-usedx1, and (C) 0.5Pt/10ZrAl-usedx1-10h. The fitting windows are highlighted. The detailed fitting results are shown in **Table S4**.

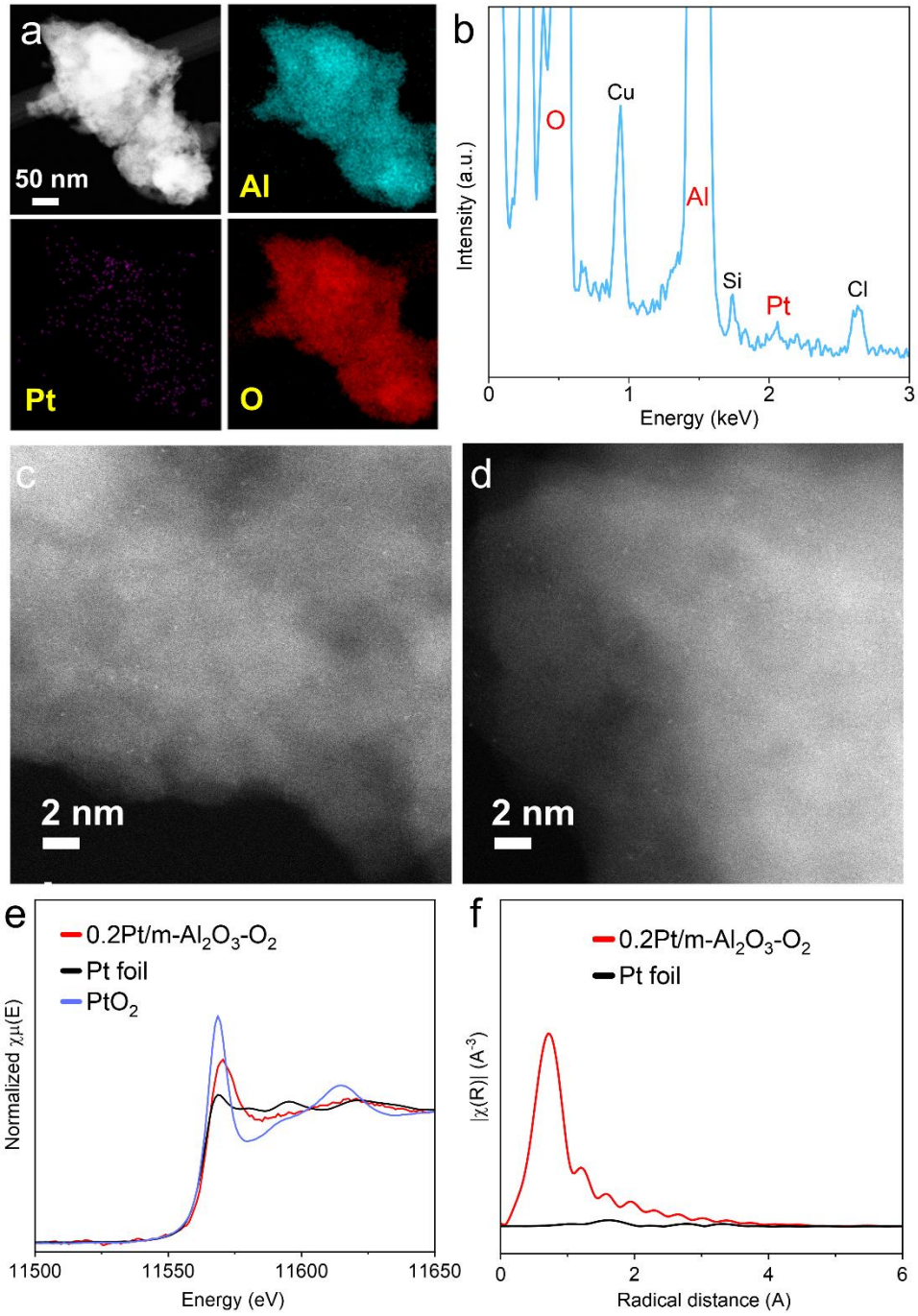

Figure S17. Characterizations of 0.2Pt/m-Al_2O_3-O_2 as the reference sample for single atom Pt catalyst. The EDS mappings (A) and corresponding sum X-ED spectrum (B) of 0.2Pt/m-Al_2O_3-O_2. The STEM-HAADF images (C, D) of atomically dispersed Pt in 0.2Pt/m-Al_2O_3-O_2. The EXAFS spectra (E) and XANES spectra (F) of 0.2Pt/m-Al_2O_3-O_2, Pt foil, and PtO_2. Detailed synthesis method please see in Ref 1.

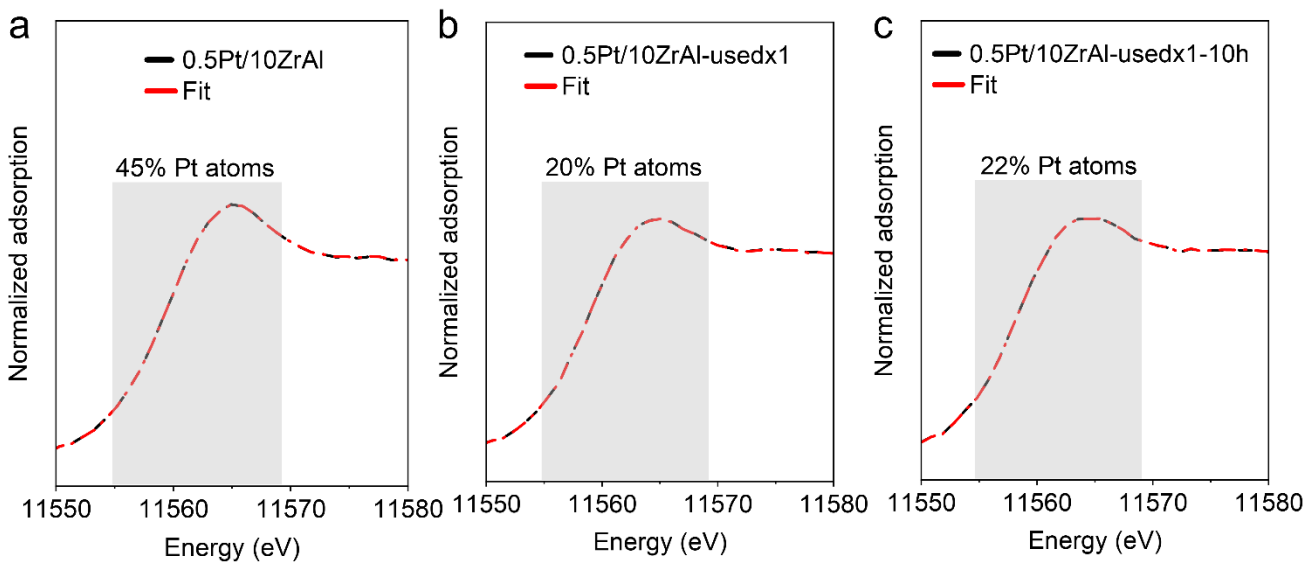

Figure S18. XANES spectra of materials and corresponding linear combination fitting curves of (A) 0.5Pt/10ZrAl, (B) 0.5Pt/10ZrAl-usedx1, and (C) 0.5Pt/10ZrAl-usedx1-10h samples. The linear combination fitting curves were fitted by using standard Pt foil and the sample with 100% Pt atoms (see in **Figure S16**). The fitting area was the grey area shown in (A-C).

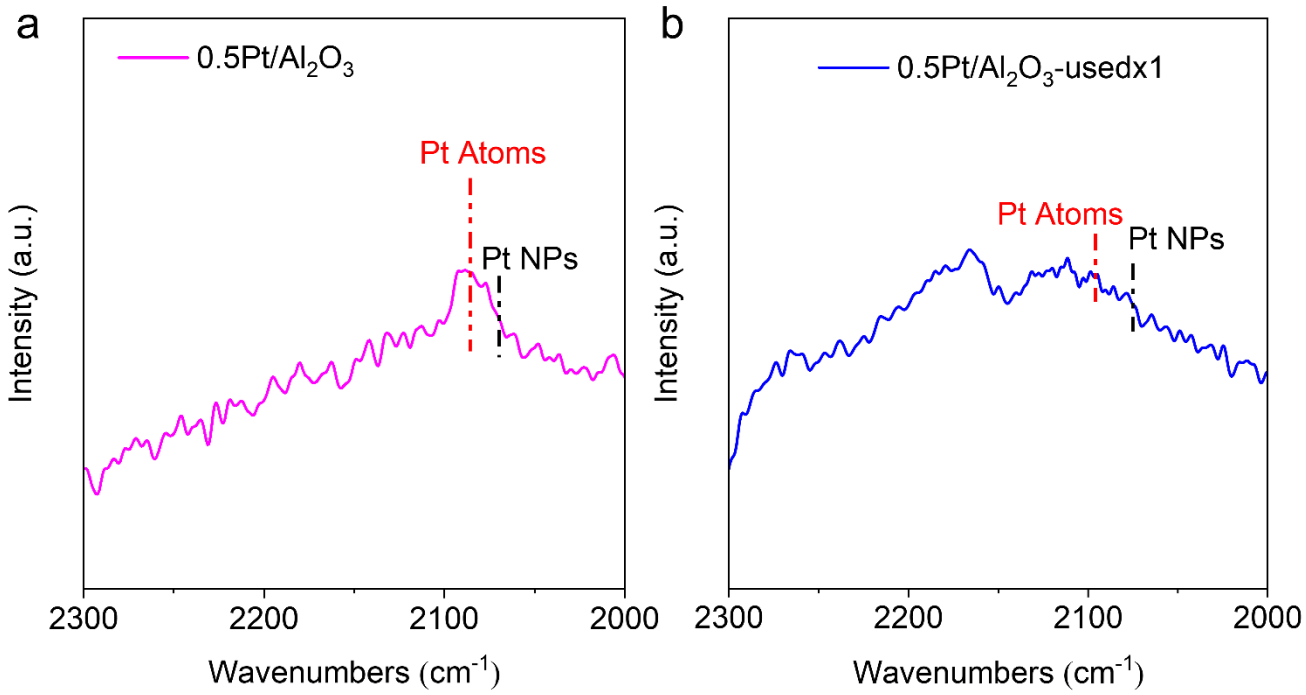

Figure S19. *In situ* CO-DRIFTS spectrums (A) 0.5Pt/Al_2O_3 and (B) 0.5Pt/Al_2O_3-usedx1. Data were collected after 5 vol.% H_2/N_2 reduction at 300°C for 60 minutes.

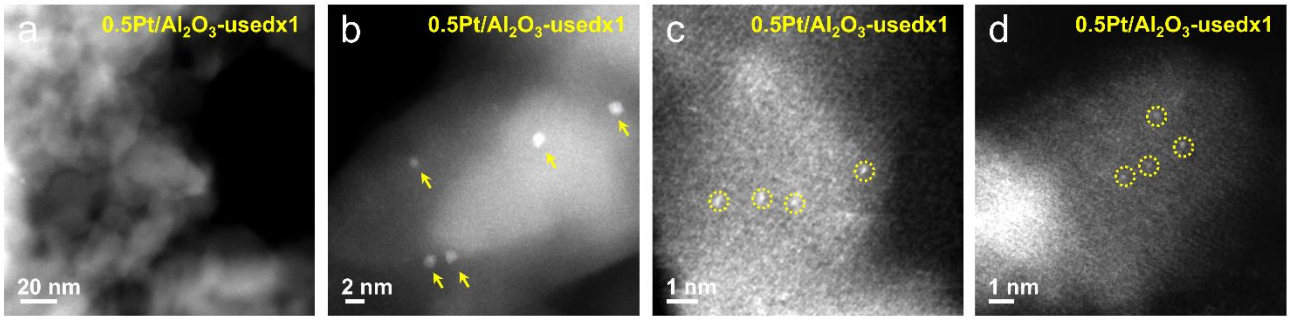

Figure S20. (A) The STEM-HAADF image of 0.5Pt/Al_2O_3-usedx1. (B) The STEM-HAADF image of Pt NPs in 0.5Pt/Al_2O_3-usedx1. (C, D) The STEM-HADDF images of Pt atoms in 0.5Pt/Al_2O_3-usedx1.

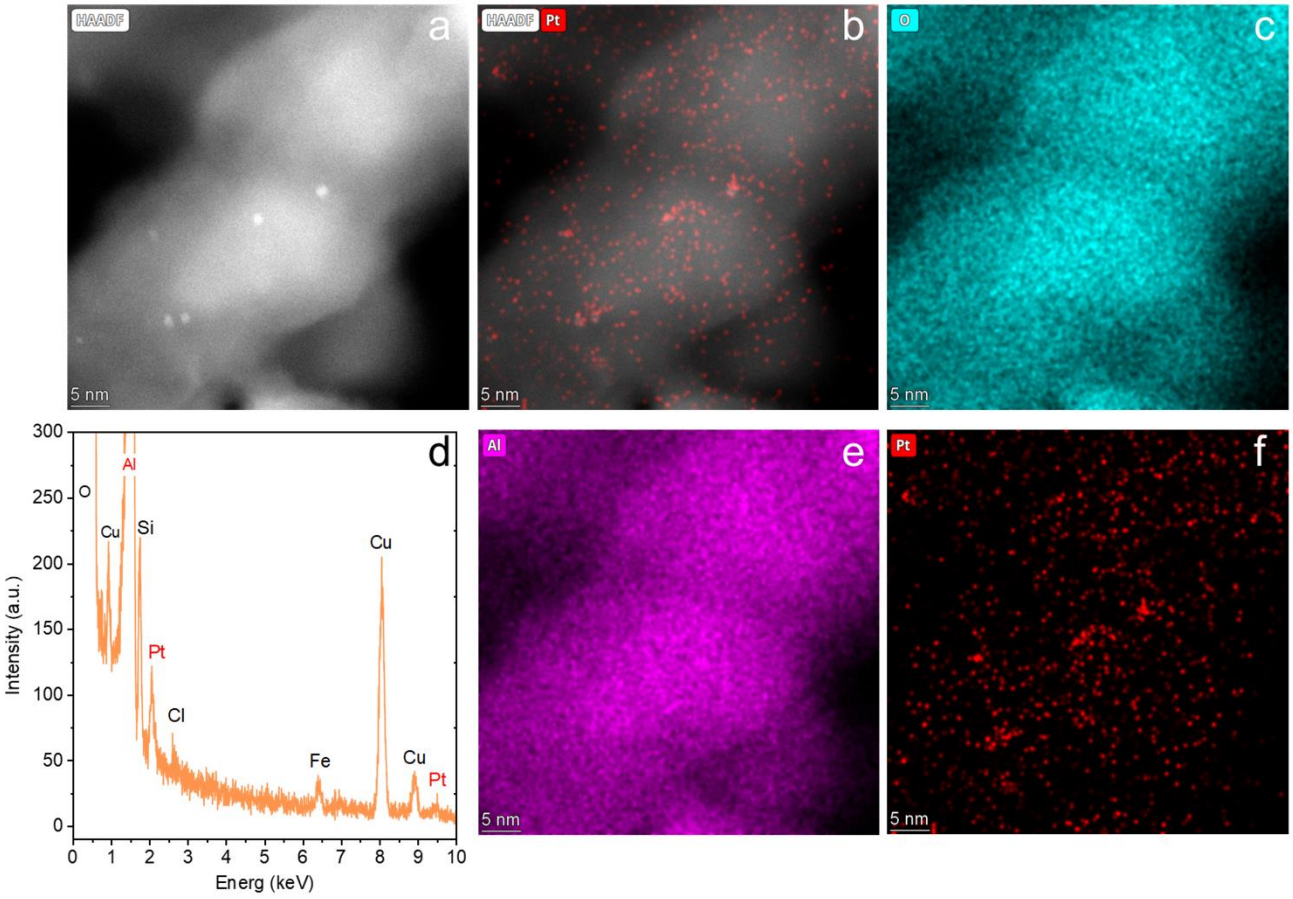

Figure S21. STEM-XEDS mappings of 0.5Pt/Al_2O_3-usedx1 and the corresponding sum X-ED spectrum, highlighting the existence of some small Pt particles. (A) The HAADF image acquired simultaneously. (B) Overlay of the Pt map and HAADF image. (C) O map. (D) Sum X-ED spectra. (E) Al map. (F) Pt map.

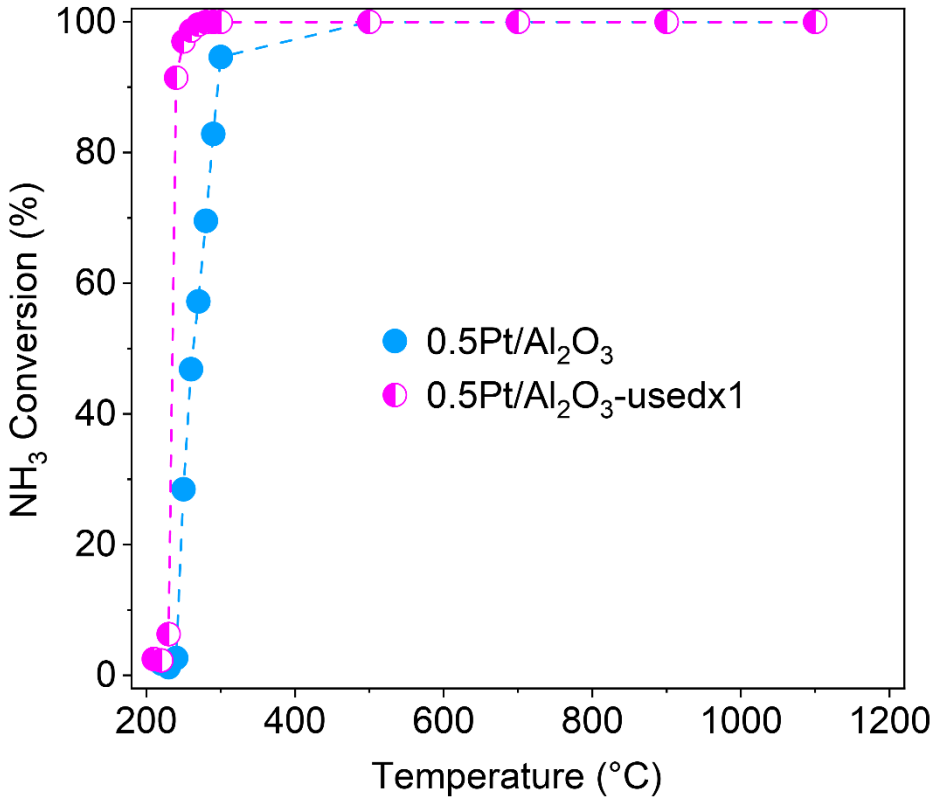

Figure S22. Light-off curves of $0.5Pt/Al_2O_3$, and $0.5Pt/Al_2O_3$-usedx1, respectively. Reaction conditions: 2 vol.% NH_3, 3 vol.% O_2, Ar balance, in total 100 mL/min, W/F_{total}= $2x10^{-3}$ (g min)/ml, GHSV= 5500 h^{-1}.

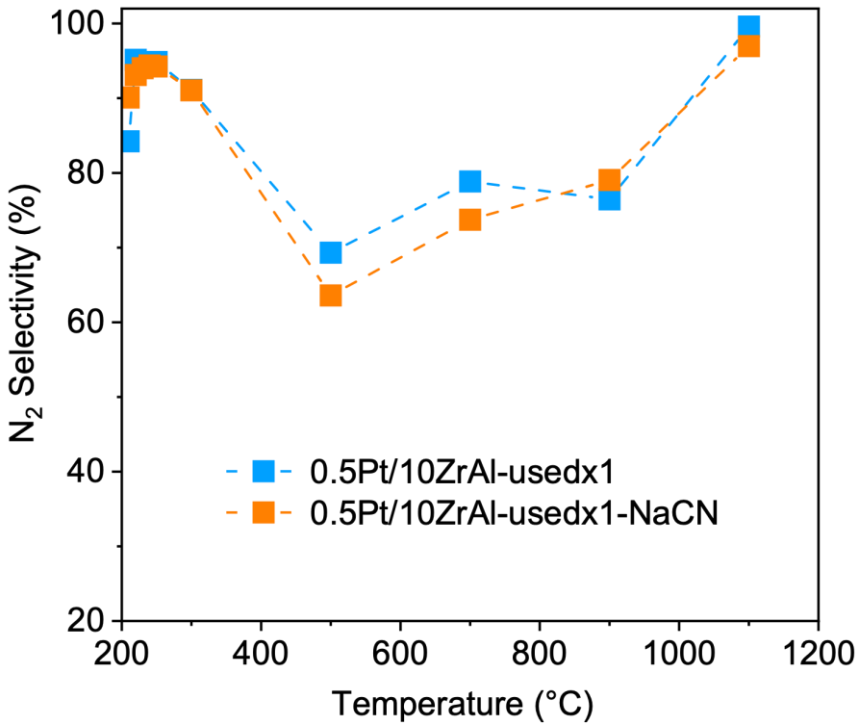

Figure S23. N_2 selectivity of 0.5Pt/10ZrAl-usedx1 before and after NaCN etched, respectively. The N_2 selectivity at 1100°C was plotted using the data measured at the 0^{th}-hour mark (minutes 0-10) when the reactor reaches target temperatures.

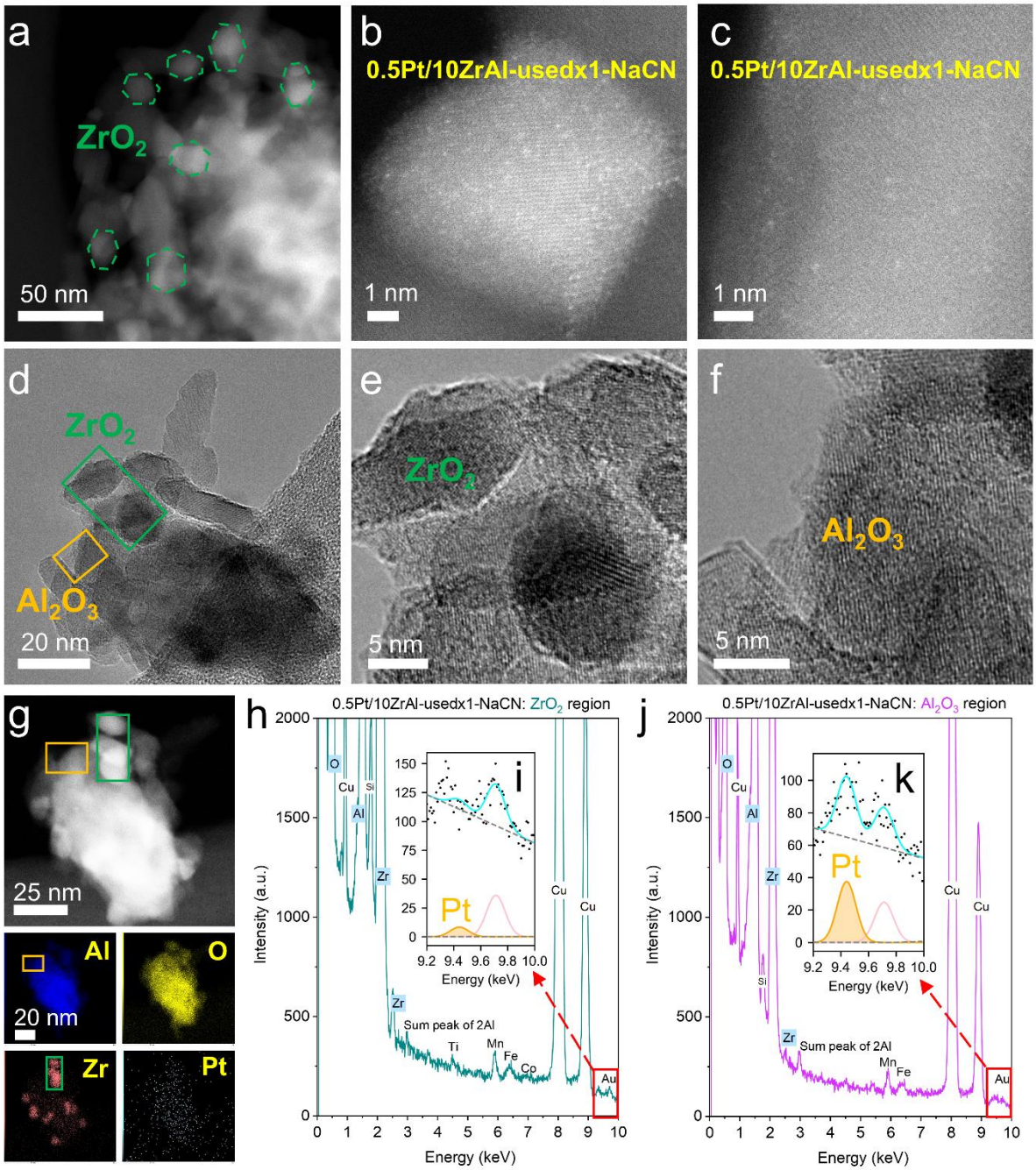

Figure S24. Electron Microscopy Characterization of 0.5Pt/10ZrAl-usedx1-NaCN. (A) STEM-HAADF image of 0.5Pt/10ZrAl-usedx1-NaCN, with magnified views of the ZrO_2-rich region (B) and the Al_2O_3-rich region (C). (D) TEM-BF image of 0.5Pt/10ZrAl-usedx1-NaCN, with magnified views of (E) the ZrO_2-rich region and (F) the Al_2O_3-rich region. (G) STEM-XEDS mappings corresponding to the TEM region are shown in (D). (H) Summed X-ED spectrum of the ZrO_2-rich region from (E), with a magnified view of the 9.2-10.0 keV range in (I). (J) Summed X-ED spectrum of the Al_2O_3-rich region from (F), with a magnified view of the 9.2-10.0 keV range in (K).

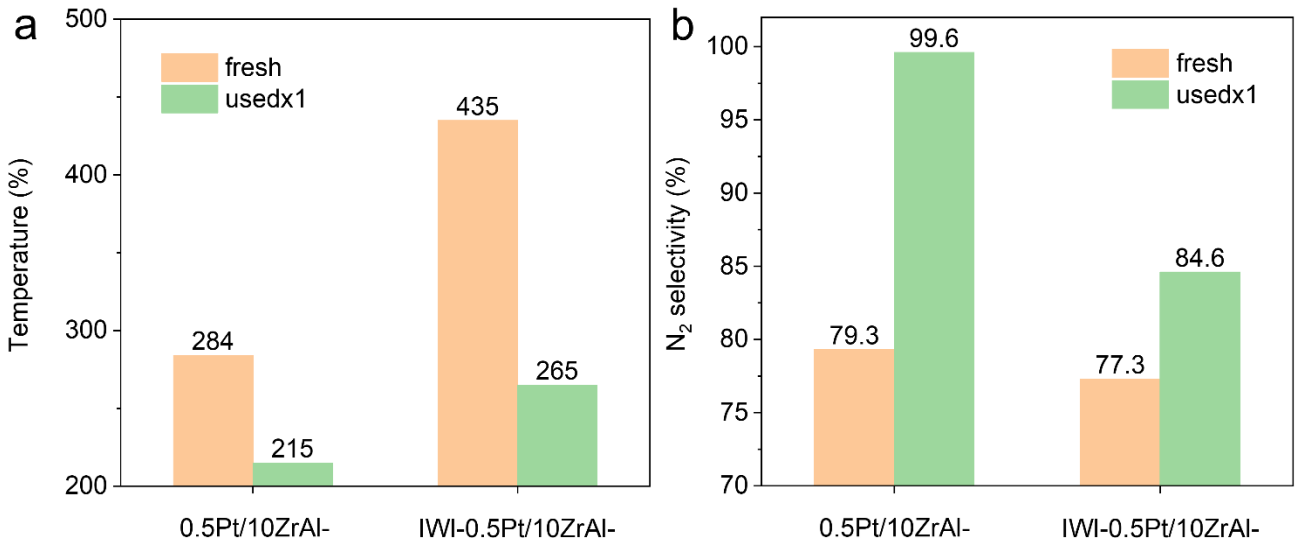

Figure S25. (A) T_{90} and (B) N_2 selectivity (1100°C) comparisons of main catalyst (0.5Pt/10ZrAl and 0.5Pt/10ZrAl-usedx1) by one-pot way, model catalyst (IWI-0.5Pt/10ZrAl and IWI-0.5Pt/10ZrAl-usedx1) by IWI way, respectively.

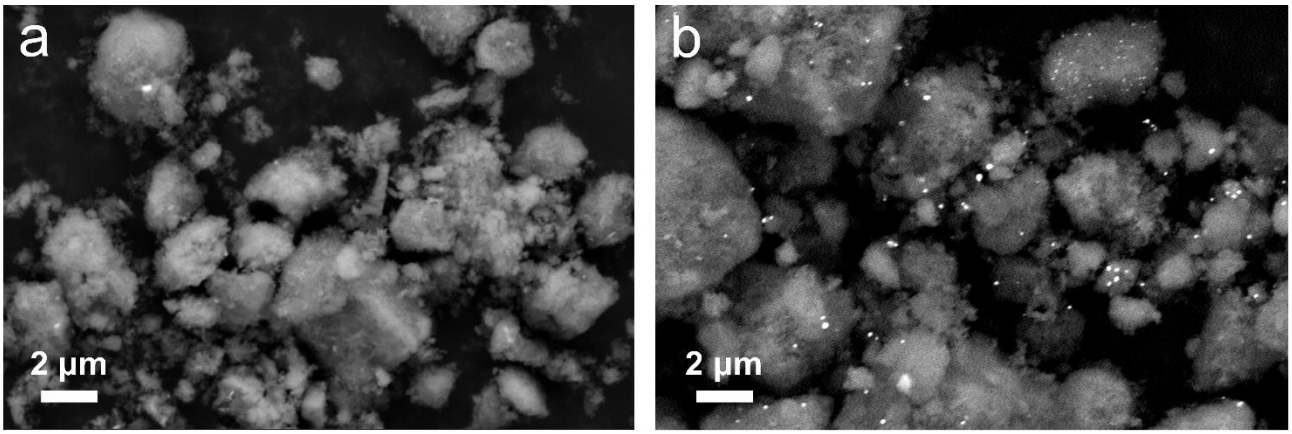

Figure S26. SEM-BSE images of (A) IWI-0.5Pt/10ZrAl and (B) IWI-0.5Pt/10ZrAl-usedx1.

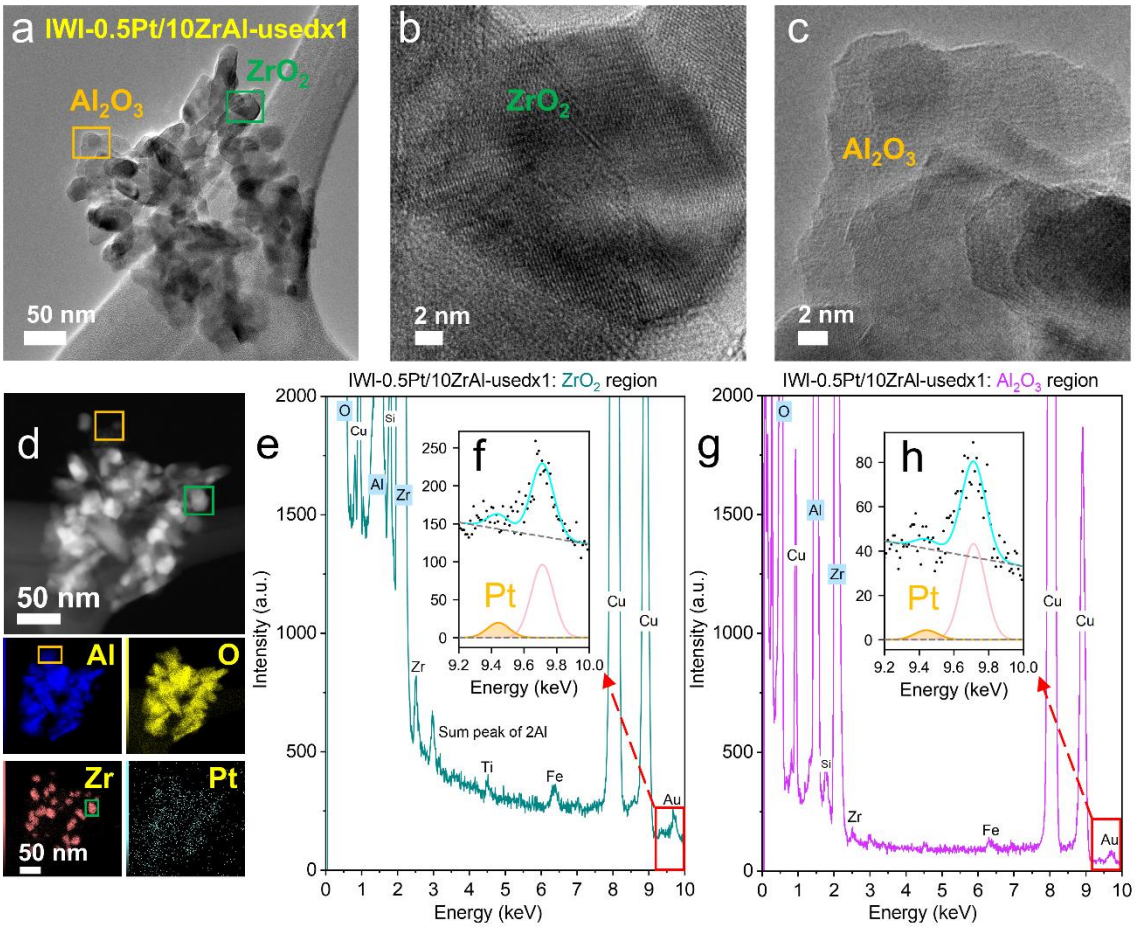

Figure S27. Characterization of IWI-0.5Pt/10ZrAl-usedx1. (A) TEM image of IWI-0.5Pt/10ZrAl-usedx1, with magnified views of the ZrO_2-rich region (B) and the Al_2O_3-rich region (C). (D) EDS mappings corresponding to the TEM region shown in (A). (E) Summed X-ED spectrum of the ZrO_2-rich region from (B), with a magnified view of the 9.2-10.0 keV range in (F). (G) Summed X-ED spectrum of the Al_2O_3-rich region from (C), with a magnified view of the 9.2-10.0 keV range in (H).

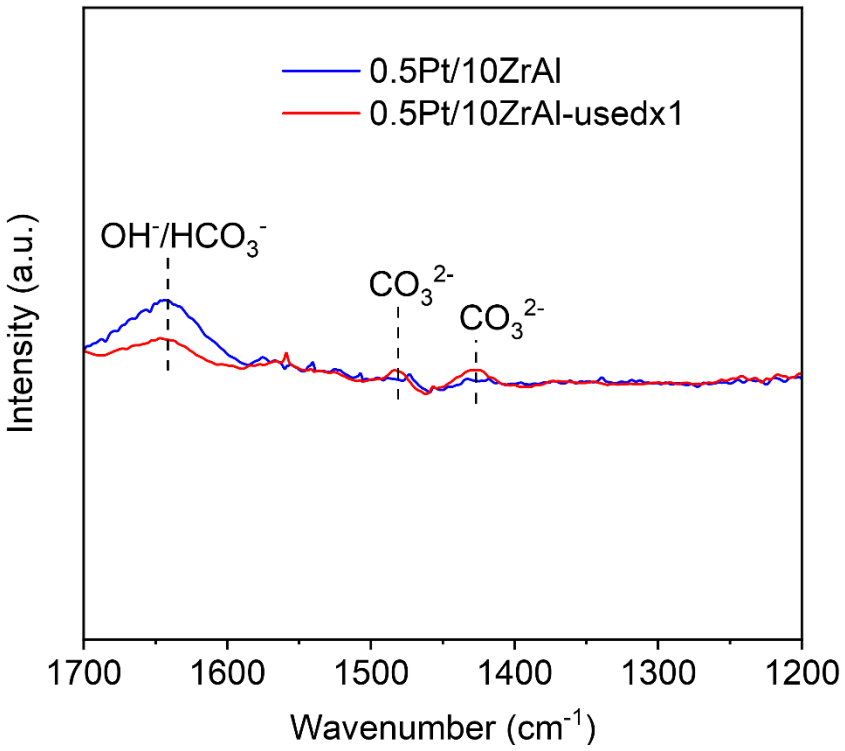

Figure S28. *In situ* CO-DRIFTS spectra of 0.5Pt/10ZrAl and 0.5Pt/10ZrAl-usedx1 at 50°C. The spectra were recorded after the samples were subjected to in situ heat treatment with 5 vol.% H_2/N_2 at 300°C for 60 minutes, following the method described in Ref 2.

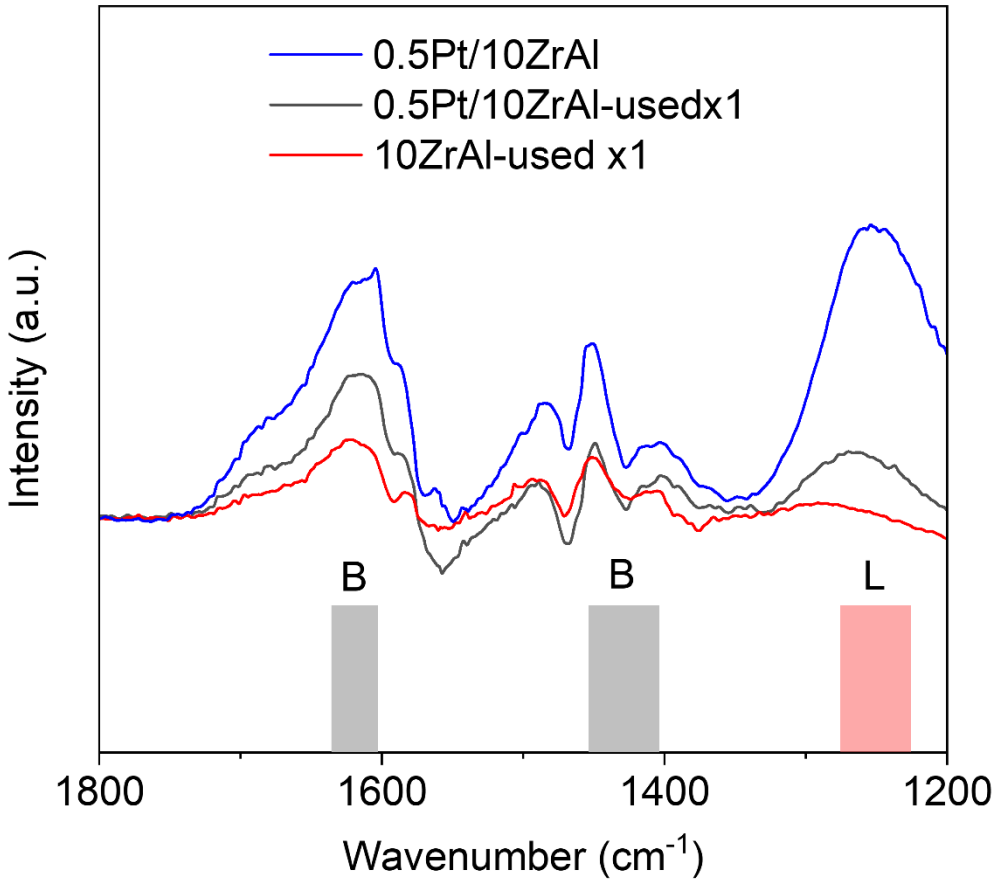

Figure S29. *In situ* DRIFTS of NH_3 adsorption at 50°C on 0.5Pt/10ZrAl, 0.5Pt/10ZrAl-usedx1, and 10ZrAl-usedx1. The Lewis and Bronsted acid sites are presented in different colors.

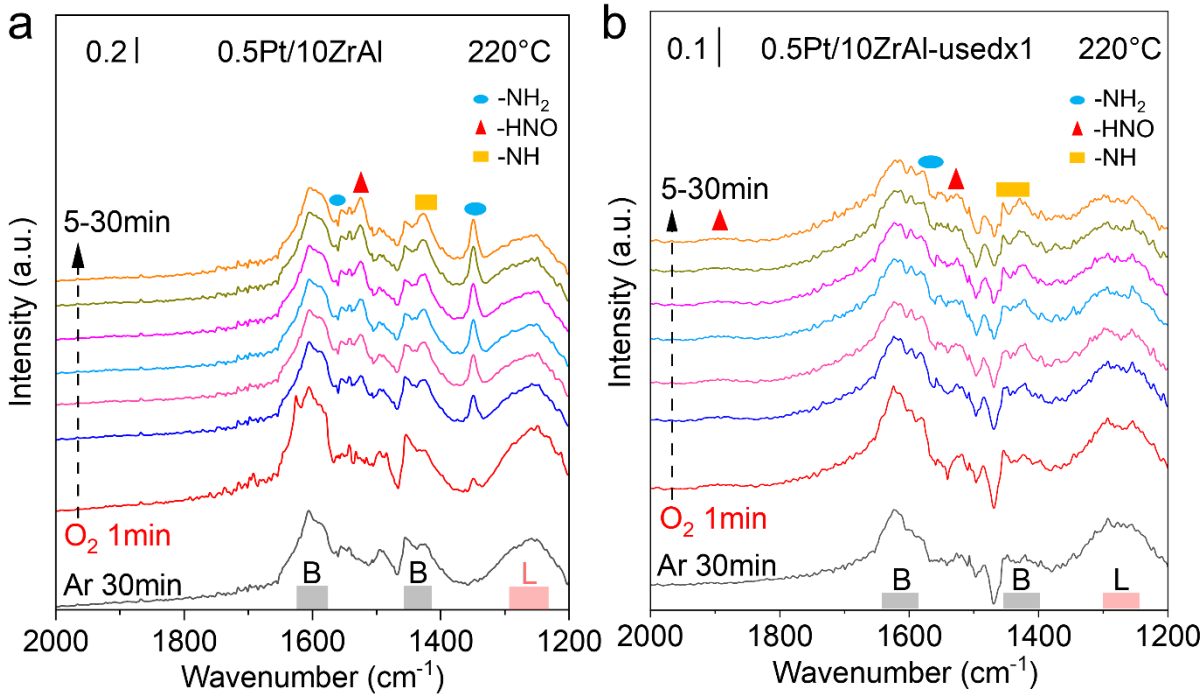

Figure S30. Detailed *in situ* NH_3-DRIFTS results for 0.5Pt/10ZrAl catalysts at 220°C. Reactivity of adsorbed NH_3 species with 3 vol.% O_2 at 220°C over 0-30 minutes for (A) fresh 0.5Pt/10ZrAl and (B) 0.5Pt/10ZrAl-usedx1 catalysts. The contributions of Lewis acid sites, Brønsted acid sites, $-NH_2$, -NH, and -HNO species are highlighted in distinct colors. Reaction conditions: 2 vol.% NH_3 or 3 vol.% O_2 in an Ar balance, with a total gas flow of 100 mL/min.

Reference

1. Zhang, Z., Zhu, Y., Asakura, H., Zhang, B., Zhang, J., Zhou, M., Han, Y., Tanaka, T., Wang, A., Zhang, T., and Yan, N. (2017). Thermally stable single atom Pt/m-Al_2O_3 for selective hydrogenation and CO oxidation. Nat. Commun. *8*, 16100.
2. Pokrovski, K., Jung, K.T., and Bell, A.T. (2001). Investigation of CO and CO_2 adsorption on tetragonal and monoclinic Zirconia. Langmuir *17*, 4297-4303.